Self-consistent analytical model of the Rayleigh-Taylor instability in inertial confinement fusion

J. Sanz
Escuela Técnica Superior de Ingenieros Aeronáuticos, Universidad Politécnica de Madrid, Madrid 28040, Spain
(Received 27 June 1995)

The model presented overcomes past inconsistencies by applying matching asymptotic techniques. The obtained growth rate, $\gamma \approx \alpha(k)\sqrt{kg} - 2k v_a$ (where v_a is the ablation velocity), could reproduce numerical simulations and experiments in a more complete way than the Takabe formula [Phys. Fluids **28**, 3676 (1985)] $\gamma = 0.9\sqrt{kg} - 3k v_a$. Here $\alpha(k) \equiv [1-(k/k_c)^r]^{1/2}$, represents the stabilization heat conduction effect and the cutoff wave number k_c is much smaller than the inverse of the density scale length at the ablation front. Such a rigorously derived stabilization mechanism clarifies many of the numerical, analytical, and simulation results found in the literature.

PACS number(s): 52.35.Py, 52.40.Nk

I. INTRODUCTION

The Rayleigh-Taylor instability (RTI) [1] in inertial confinement fusion (ICF) is critical for the achievement of appropriate implosions. In the direct drive approach, laser beams simultaneously illuminate the outer surface of a spherical capsule. In indirect drive, lasers or ion beams first convert to x rays inside a high-Z enclosure (hohlraum target), which then drives the implosion. Regardless of the approach, a low-density plasma blowoff accelerates a higher density pusher radially inwards at the ablation front, and this is the standard situation for the occurrence of the Rayleigh-Taylor instability [2]. Since 1974, the RTI in ICF has been the goal of arduous theoretical as well as numerical or experimental work. The theoretical knowledge of the different physical mechanisms involved and the scaling laws are fundamental. In 1974, Bodner [3] reported a simple discontinuity model of such instability, however, he needed to introduce an "*ad hoc*" assumption to close the problem. He found that the growth rate γ could be reduced below the classical value ($\sqrt{kg}$) due to mass ablation and described it as $\gamma \approx \sqrt{kg} - k v_a$, where k is the transverse wave number, v_a is the flow velocity across the ablation front, and g the target acceleration. All the numerical simulations [4] and experimental results [5] that followed suggested larger stabilization effects.

Numerous attempts have been made to develop an analytical model by means of a surface discontinuity (ablation surface) separating two uniform fluids [6]. Since this approach leaves the solution undetermined, other approximations circumvent these difficulties either by including in the analysis a layer with a diffuse boundary centered at the ablation front (with a thickness of order of the density gradient scale length) and solving numerically a linearized eigenvalue problem [7–9], or by using a WKB model [10] (assuming very small wavelength perturbations).

Although the general belief is that the reduction is due to mass ablation, the single *theoretical support* for such a large stabilization is the so-called Takabe formula [7]:

$$\gamma = 0.9\sqrt{kg} - 3k v_a \ , \tag{1}$$

which was obtained by means of a *numerical fitting* and it is repeatedly referenced in the literature. Laser fusion simulations seem to agree well with this formula, however, a recent set of indirect-drive experiments conducted on the Nova laser [11] could suggest a not so large stabilization ablative effect [factor 3 Eq. (1)].

It is well known that flow expanding through an interface may require additional information besides the conservation relations across it [12]. Obtaining these additional conditions has been the most speculative part of the models about RTI in ICF and a recurrent inconsistency for the last 20 years; all this becomes worse by the extra difficulty of approximating the near hot plasma corona region, dominated by the inhomogeneity of the fluid, in a realistic way. The model presented here overcomes this obstacle by considering on the one hand the inner structure of a thin transition layer (ablation surface), as in studying the stability of slow-combustion fronts [13], and on the other hand by performing, in a rigorous way, an asymptotic matching (no jump conditions) to both sides of it [14]. The result that is obtained is independent of the type of driver (direct or indirect) and also of the physical details about the form in which energy is absorbed. The application of the matching asymptotic technique to RTI in ICF is a novelty, and the first results already have been published [15]; the main stabilization mechanism found is due to the overpressure produced by heat conduction and such a stabilization mechanism underlies many of the numerical, analytical, and simulation results. In the work that we are presenting here, additional results are shown explaining to a large extent the technique that is carried out. The soundness of the physical model is based both on the assumption of a sharp ablation front and on the smallness of Mach number of the flow through it.

In the rest of this section we present the general equations, a discussion about the different lengths and characteristic times of the hydrodynamics, and a brief review of the boundary conditions used in the past. In Sec. II the analysis of the problem is carried out. In Sec. III the

dispersion relation is discussed. Section IV is dedicated to different comparisons and Sec. V to conclusions.

A. General equations: Lengths and characteristic times of the hydrodynamics

In order to obtain physical insight into the analysis of the problem, it is basic to discuss in terms of the physical parameters, lengths and characteristic times of the different regions and their comparison. For simplicity, we are considering a planar foil of thickness l (small compared with the ablation radius r_a of the shell if spherical), which is moving with an acceleration g due to the ablation pressure $p_a \approx \rho_{\rm av} l g$ ($\rho_{\rm av} \equiv$ slab average density), generated by the heat flux coming from the corona. This slab is continuously ablating with a mass ablation rate $\dot{m}$.

We use the same one-fluid equations as Bodner [3] (in the frame moving with the unperturbed ablation front), but we do not assume incompressibility and moreover the heat conduction is explicitly taken into account:

$$\partial\rho/\partial t + \nabla\cdot(\rho \mathbf{v}) = 0 \ . \tag{2}$$

$$\partial(\rho \mathbf{v})/\partial t + \nabla\cdot(\rho \mathbf{v}\mathbf{v}) = -\nabla(\rho T) + \rho \mathbf{g} \ , \tag{3}$$

$$\partial/\partial t(\rho v^2/2 + 3\rho T/2) + \nabla\cdot[\rho \mathbf{v}(5T/2 + v^2/2) - K\nabla T] = \rho \mathbf{v}\cdot\mathbf{g} \ . \tag{4}$$

We also assume the fluid to be a monatomic perfect gas, the temperature is conveniently normalized (measured in energy per unit mass units), $\mathbf{g} = g\mathbf{e}_x$ and K is the thermal conductivity. Equation (4) does not contain an energy deposition term, for instance, by means of laser energy, because the absorption region is located at a large distance from the ablation surface compared with the wavelength perturbations we are considering. The thermal conductivity is assumed to have a power law dependence on the temperature and the density, $K = \bar{K} T^{n-\mu}/\rho^{\mu}$, $1 < \mu < 2$, $5 < n < 8$ [16], in order to roughly describe other possible transport energy mechanisms, such as radiation. In Laser fusion and for electronic heat conduction we have $\mu \equiv 0$ and $n = 5/2$ [17].

One can distinguish three asymptotic regions to be matched (see Fig. 1): (i) a cold and adiabatically compressed zone (region 1) of thickness l, which presents a maximum of the density ρ_a, where its values for the pressure and temperature are p_a and T_a, respectively; (ii) an adjacent thin layer (region 2), where the material is being heated and expanding towards the corona, the pressure is approximately constant, $\rho T \approx p_a$, but not the density, which is of the order of magnitude of ρ_a; the characteristic thickness Δ of region 2 (approximately equal to the gradient scale length at the ablation front) [8], which is obtained by means of a simple energy balance $\dot{m} T_a \sim \bar{K} T_a^{n+1-\mu}/(\rho_a^{\mu}\Delta)$, is defined as

$$\Delta \equiv \frac{\bar{K} T_a^{n-\mu}}{\dot{m}\rho_a^{\mu}} \ . \tag{5}$$

The characteristic Mach number of the flow velocity, $M_a \equiv v_a / \sqrt{p_a/\rho_a}$, is assumed to be a small parameter,

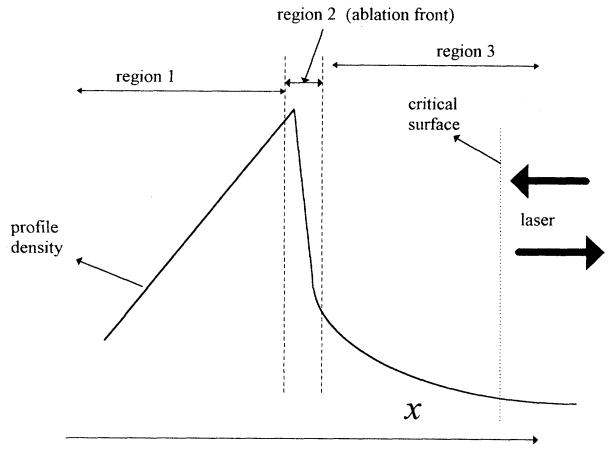

FIG. 1. Schematic profile of density.

with $v_a \equiv \dot{m}/\rho_a$ defining the ablation velocity. (iii) Finally, the hot plasma corona (region 3) where the flow reaches sonic conditions and the order of magnitude of the characteristic density $\rho_{\rm cor}$, velocity $v_{\rm cor}$, temperature $T_{\rm cor}$, and the layer thickness L are estimated in a simple way through mass, momentum, and energy balance:

$$\rho_{\rm cor} v_{\rm cor} \sim \dot{m} \ , \qquad \rho_{\rm cor} v_{\rm cor}^2/L \sim \rho_{\rm cor} T_{\rm cor}/L \sim p_a/L \ , \tag{6}$$

$$5\rho_{\rm cor} v_{\rm cor} T_{\rm cor}/2 \sim \bar{K} T_{\rm cor}^{n+1-\mu}/(\rho_{\rm cor}^{\mu} L) \ , \tag{7}$$

then we get

$$\rho_{\rm cor} \equiv \rho_a M_a^2, \quad T_{\rm cor} \equiv v_{\rm cor}^2 \equiv \left[\frac{p_a}{\dot{m}}\right]^2 , \qquad L \equiv \left[\frac{p_a}{\dot{m}}\right]^{2n} \frac{2\bar{K}}{5n\dot{m}p_a^{\mu}} \ , \tag{8}$$

where the factor n, appearing in the denominator of the formula for L, has been introduced for convenience. Thus, one can obtain, using Eq. (5), a relation between the characteristic lengths of regions 2 and 3:

$$L = \frac{2\Delta}{5nM_a^{2n}} \ , \tag{9}$$

and therefore, since usually $M_a \ll 1$, the characteristic length of region 3 is much larger than the characteristic length of region 2. We will also assume the target thickness l such that $\Delta \ll l \ll L$, which may correspond to a reasonable typical configuration in ICF.

Let us suppose that the order of magnitude of the characteristic time of the duration of the process is that of the existence of the target until it is evaporated totally, $t_e \approx \rho_a l/\dot{m}$. The RTI is developed in a characteristic time $\gamma_{\rm cl}^{-1} \equiv (\sqrt{kg})^{-1}$. Attention is restricted to instability wave numbers $k > 1/l$ because the stabilization occurs, as will be proved shortly, for such wave numbers [$kl \sim (kL)^{1/n}$ in the limit $M_a \to 0$], and therefore, the equilibrium does not change on the time scale of the

growth rate, $\gamma_{\rm cl} t_e \gg 1$, so a perturbation analysis of the type $\propto e^{\gamma t}$, where γ is the time growth rate of the instability, may be carried out. Typical targets could have ratio l/L values such that $k v_a^2/g \sim klM_a^2 \sim (kL)^{1/n} M_a^2 \ll 1$ (main assumption of the model), and therefore using Eq. (9) we obtain $k\Delta \ll 1$. For instance, the simulations performed by Gardner, Bodner, and Dahlburg [4] have $klM_a^2 \sim 0.04$.

In order to prove the occurrence of that stabilization mechanism for such wave numbers, let p_*, v_*, and T_* denote the characteristic pressure, velocity, and temperature, respectively, at a distance k^{-1} from the ablation surface inside region 3, and let us also assume $\Delta \ll k^{-1} \ll L$. Then using mass, momentum, and energy conservation we get

$$\rho_* v_* \sim \dot{m}, \quad p_* - p_a \sim -\dot{m} v_*, \quad \dot{m} T_* \sim \frac{\bar{K} T_*^{n+1}}{k^{-1} p_*^{\mu}} ; \tag{10}$$

therefore one can obtain

$$v_* \sim \dot{m}/\rho_* \sim v_{\rm cor} (kL)^{-1/n}, \quad T_* \sim T_{\rm cor} (kL)^{-1/n} , \qquad p_* - p_a \sim -p_a (kL)^{-1/n} . \tag{11}$$

If p_{a1} is the perturbed ablation pressure due to the deformation x_a of the rippled ablation front with wave number k ($kx_a \ll 1$), using the last of Eq. (11) we obtain

$$p_{a1} \sim k x_a p_a (kL)^{-1/n} . \tag{12}$$

Then, the heat conduction causes the pressure to increase on the crest of the rippled ablation front and to decrease on the valley, damping the growth. Now, using a mechanical balance [18] and $p_a \sim \rho_a g l$, one can obtain, apart of numerical factors,

$$\frac{\partial^2 x_a}{\partial t^2} \sim kg \left[1 - \frac{kl}{(kL)^{1/n}} \right] x_a . \tag{13}$$

Certainly, the convection of the material through the interface would also damp the growth and, in some cases, both effects could be numerically comparable.

B. Brief review of the different boundary conditions used in the past

The use of a model with a discontinuity surface is a physically reasonable assumption if the wavelength of the disturbances is large compared with the characteristic thickness of region 2, $k\Delta \ll 1$ (so region 2 compared with regions 1 and 3 becomes a surface), though in a recent work [9] the authors supposed unnecessarily $kL \ll 1$, and such a condition is much more restrictive. The difficulties presented by the discontinuity surface approximation in the study of RTI in ICF are numerous. The thermal flow in region 1 is negligible, in region 3, to the contrary, it is basic to consider it, even for disturbances with large wavelength, $kL \ll 1$, opposite to what occurs in the study of the stability of a flame [13]; not to retain this effect can lead to questionable conclusions when the comparison between both problems is carried too far (for instance, the boundary condition of Landau-Darrieus in the stability of a flame front cannot be applied to ICF). To connect regions 1 and 3 the use of conservation laws is not enough; one must study partially the structure of region 2 and an asymptotic matching of the region 3 solution to the one that emerges from region 2 is necessary. The peculiar behavior of the density, temperature, and velocity near the ablation surface from the side of the corona causes every attempt that uses patching or purely jump conditions in a standard way through the interface to fail. We should note that, as indicated already by Manheimer and Colombant [6], the values of the unperturbed variables, just behind the ablation surface, are not well defined. The puzzle of the boundary conditions coming all the way from Bodner [3], and which we briefly summarize in this section, can be clarified if on the one hand the more basic (in the limit $k\Delta \to 0$) structure of region 2 and the nearest hot plasma of region 3 (considering the heat flux) are held and on the other hand an asymptotic matching of both regions is carried out [14], which is rigorously necessary in order to connect regions 1 and 3 without ambiguities.

All the models in the past have considered a uniform fluid to each side of the surface discontinuity and, in particular on the side of region 3. Then, the perturbations obey a system of ordinary differential equations of constant coefficients whose solutions are of the type $\exp(qx + iky + \gamma t)$, where x and y are the coordinates along the main flow and the unperturbed front, respectively. The number of modes depends on the physical effects that the equations are taking into account: commonly they are four modes (four roots q) for incompressible and adiabatic flows and five for the flows with thermal conduction; to these, one must add one mode more, the mode corresponding to the deformation of the front $\xi \exp(\gamma t + iky)$. Only those modes with $\mathrm{Re}(q) > 0$ as $x \to -\infty$ and $\mathrm{Re}(q) < 0$ as $x \to +\infty$ are physically allowed.

1. *Flows without thermal conduction to both sides of the discontinuity*

In this case if γ is assumed a real number, there are four real roots q; three of them are positive and a fourth is negative, hence we should determine five modes: the only mode that does not explode in the prefront region, the three modes that do not explode in the postfront region, and finally the corresponding mode to the perturbed front $\xi \exp(\gamma t + iky)$. Five boundary conditions are necessary to obtain the dispersion relation.

In Ref. [3], Bodner used the mass and momentum conservation laws (along the directions x and y) through the interface, and he introduced two *ad hoc* boundary conditions in order to close the problem: energy conservation through the interface with an arbitrary source term, which is related to the deformation of the interface and (the fifth boundary condition is the one that relates) through an arbitrary constant, the perturbed pressure just before the front to its deformation.

Book [19] used a very similar model, except that he did not consider any source term in the energy conservation

equation and he assumed another relation between the perturbed pressure just before the front and its deformation. Baker [6] assumed as additional boundary condition the fact that the perturbed density vanishes just behind the front. Bychkov, Golberg, and Liberman [9] used, for their regime of large wavelength, the Landau-Darrieus boundary condition [20], which expresses that the prefront velocity is unchanged. Recently, Wouchuk and Piriz [21] presented a model that is closed by means of a phenomenological and modified version of the Landau-Darrieus boundary condition [22].

We indicate here that a self-consistent model would have to consider some energy source term in the energy equation, as in fact only Bodner [3] and Baker [6] have considered. The omission of such a source term in the conservation energy law through the ablation front is incompatible with a jump of density.

2. *Flows with thermal conduction*

Manheimer and Colombant [6] used a model where they neglected the heat flux in the prefront region, which then has one bounded mode to be determined, and a postfront region with thermal conduction (a fifth-order differential linear system for the perturbations) that contains three bounded modes if the flow is subsonic and four if supersonic. Then, in addition to the four boundary conditions that are obtained from the conservation laws through the interface (mass conservation, two of momentum conservation and one of energy conservation), one or two additional boundary conditions are needed if the flow is subsonic or supersonic, respectively. For supersonic flow the authors imposed that the perturbed density and temperature vanish just behind the front. While for subsonic flow they used a phenomenological law about the generation of vorticity at the interface.

Kull and Anisimov [6] assumed thermal conduction to both sides of the interface and subsonic flow everywhere, so that there are two possible modes in the prefront region and three in the postfront. To connect both regions they imposed, in addition to the four conditions that are obtained from the usual conservation laws, a fifth boundary condition obtained integrating twice the energy equation and finally, to close the problem, they assumed, as the sixth condition, that the interface deformation was null.

In order to clarify this set of boundary conditions let us point out the following physical aspects of the problem. In the long wavelength regime, that is to say greater than the distance between the ablation and the critical surfaces, this region can be dealt with as a discontinuity surface. In the postfront region the flow is supersonic and, as Manheimer and Colombant showed [6], four bounded modes are possible. The assumption of the fact that this region is subsonic, with three bounded modes instead of four, as Bychkov, Golberg, and Liberman [9] supposed in their work, is then questionable. The two additional boundary conditions are as follows: one of them is the same as that which Manheimer and Colombant supposed; we mean the perturbed density just behind the front (where we have the critical density) must be zero. The second boundary condition, which Manheimer and Colombant did not know how to find (they assumed the temperature to vanish just behind the front), comes from the fact that the flow necessarily has to cross an isothermal sonic point, the one that is a singular point of the equations. See, for example, the complete discussion of Ref. [23]. Finally, in the regime that Manheimer and Colombant call the subsonic flow, $\Delta \ll k^{-1} \ll L$, the approach of the problem must be different: the structure of the thermal wave that is established in that region, and whose foot defines the ablation surface, is basic as well as the determination in part of the structure of region 2, whose characteristic thickness is Δ, and the matching asymptotic technique must be used.

It would be interesting in order to clarify the situation to make a qualitative study of the different modes that can take place in the prefront and postfront regions. For simplicity in the discussion we suppose the flow is subsonic, so that the dynamic pressure is small compared with the thermal one, and therefore an isobaric approximation is a reasonable assumption. The fluid, however, is not incompressible since the heat flux modifies considerably the temperature and therefore the density $\rho \approx p_a / T$. We also assume the derivatives of the unperturbed solution are negligible. Let $\rho_1 \approx -\rho_0 T_1 / T_0$, $\boldsymbol{v}_1$, and p_1 denote the perturbed density, velocity, and pressure, respectively, which verify the following equations:

$$(\partial/\partial t + v_0 \partial/\partial x)(\rho_1/\rho_0) \approx -\nabla \cdot \boldsymbol{v}_1 , \tag{14}$$

$$(\partial/\partial t + v_0 \partial/\partial x)\boldsymbol{v}_1 \approx -\nabla p_1 + \rho_1 \mathbf{g} , \tag{15}$$

$$\nabla \cdot \boldsymbol{v}_1 \approx -\tfrac{2}{5} \Delta_0 \nu_0 \nabla^2 (\rho_1/\rho_0) , \tag{16}$$

where $\Delta_0 \equiv (T_0/T_a)^n \Delta$. For wave number perturbations such that $k\Delta \ll 1$, the thermal conduction in region 1, where $T_0 \sim T_a$, is negligible. The opposite must occur in region 3, where $T_0 \gg T_a$, and at distance $x \sim k^{-1}$ from the ablation surface we have $k^{-1} \sim \Delta_0$ (notice that $T_0/T_a \sim x^{1/n}$) and consequently, the thermal conduction is not negligible in this region. For perturbations of the type $\exp(qx + iky + \gamma t)$, in region 1, with $\nabla \cdot \boldsymbol{v}_1 \approx 0$, the corresponding roots to the four modes are $q \approx -\gamma / v_a$, which is double (corresponding to the vorticity and the entropy modes) and $q \approx \pm k$ (corresponding to the potential incompressible flow modes). The fifth mode, which is strictly not null and corresponds to the heat diffusion, decays very quickly with the distance ($q \sim \Delta^{-1}$) and, except in a very narrow region such as region 2, its effect can be neglected. In region 3, the five modes have the following roots for $kx \gg 1$: $q \approx -\gamma / v_0$ (vorticity mode) and the double roots $q \approx \pm k$, two of them ($\pm$) correspond to the heat diffusion and the other two correspond to the potential incompressible flow (or sound) modes.

II. ANALYSIS OF THE REGIONS

We look for solutions of perturbed quantities of the form $\exp(\gamma t + iky)$. Let $x = 0$ be the unperturbed position (with a precision of the order of Δ) of the ablation front and $x_a \approx \xi \exp(\gamma t + iky)$ its perturbation (in the lim-

it $k\Delta \to 0$ region 2, compared with regions 1 and 3, becomes a surface discontinuity). It is convenient to strain the x coordinate [14] defining a new variable in the form $s = x - x_a$. Then, the partial derivatives are changed in the following way:

$$\frac{\partial}{\partial t} \to \frac{\partial}{\partial t} - \frac{\partial x_a}{\partial t}\frac{\partial}{\partial s}, \quad \frac{\partial}{\partial x} \to \frac{\partial}{\partial s},$$
$$\frac{\partial}{\partial y} \to \frac{\partial}{\partial y} - \frac{\partial x_a}{\partial y}\frac{\partial}{\partial s} .$$

We also expand the velocity $\mathbf{v}$, density ρ, and temperature T:

$$\mathbf{v} = v_{1y}(s)\exp(\gamma t + iky)\mathbf{e}_y + \{v_0(s) + [v'_{1x}(s) + \gamma\xi]\exp(\gamma t + iky)\}\mathbf{e}_x , \quad (17)$$

$$\rho = \rho_0(s) + \rho_1(s)\exp(\gamma t + iky) , \quad (18)$$

$$T = T_0(s) + T_1(s)\exp(\gamma t + iky) . \quad (19)$$

Notice that v'_{1x} is the velocity with respect to the moving perturbed ablation surface, which is located at $s = 0$. Though the unperturbed variables have been expressed as only functions of the coordinate s, they actually could depend on time, but in a slower time scale compared with γ^{-1}. We would then proceed with the analysis of Eqs. (2)–(4) in zero order and linearize in the first order perturbations. In Appendix A we show the full equations for the perturbations.

A. Analysis of region 1 (cold and adiabatically compressed zone)

In region 1 ($s < 0$), after a transient time, the flow velocity becomes very subsonic ($M_a \ll 1$) in the frame moving with the target. In general the unperturbed flow is not quasisteady in this region.

1. Unperturbed solution

Time derivatives must be retained since they are comparable to convective terms, $\partial/\partial t \sim v_0 \partial/\partial s$. We use the continuity, momentum, and the entropy equations. Notice that the heat conduction is negligible in this region, since $\rho_0 T_0 v_0 \sim \rho_a T_a v_a \gg K dT_0/ds \sim \rho_a T_a v_a (\Delta/l)$:

$$\frac{\partial \rho_0}{\partial t} + \frac{\partial(\rho_0 v_0)}{\partial s} = 0 , \quad (20)$$

$$\rho_0 \frac{\partial v_0}{\partial t} + \rho_0 v_0 \frac{\partial v_0}{\partial s} = -\frac{\partial p_0}{\partial s} + \rho_0 g , \quad (21)$$

$$\frac{\partial}{\partial t}\left[\frac{p_0}{\rho_0^{5/3}}\right] + v_0 \frac{\partial}{\partial s}\left[\frac{p_0}{\rho_0^{5/3}}\right] = 0 , \quad (22)$$

where the pressure $p_0 \equiv \rho_0 T_0$. The integration of Eqs. (20)–(22) would need in general, besides the initial conditions, the boundary conditions at the rear side of the target ($s \approx -l$); for instance, if there were vacuum or a negligible ambient pressure we will have there $v_0 \approx -dl/dt$, $p_0 = \rho_0 \approx 0$. Also we would need the boundary conditions at just before the ablation surface $s = 0^-$, $p_0 \approx p_a$, and $v_0 \approx v_a \equiv \dot{m}/\rho_a$, where both p_a and $\dot{m}$ (assumed known) depend mainly on the irradiation conditions of the target; however, ρ_a depends on the initial conditions and in general on the history of the evolution of the target. Equation (21) may be integrated since $\rho_0 g l \gg \rho_0 v_0^2$, giving us

$$p_0 \approx \int_{-l}^{s} \rho_0(s') g \, ds' , \quad (23)$$

and then

$$p_a \approx \int_{-l}^{0} \rho_0(s') g d s' \equiv \rho_{\mathrm{av}} g l , \quad (24)$$

with ρ_{av} being the slab average density. Consequently an approximate solution by expanding for $|s/l| \ll 1$, may be obtained using Eqs. (20), (22), and (23):

$$p_0 \approx p_a \left[1 + \frac{\rho_a}{\rho_{\mathrm{av}}}\frac{s}{l} + \cdots\right] , \quad (25)$$

$$\rho_0 \approx \rho_a \left\{1 + \left[\frac{\rho_a}{\rho_{\mathrm{av}}} + \frac{l}{v_a}\frac{d}{dt}\ln\left[\frac{p_a}{\rho_a^{5/3}}\right]\right]\frac{s}{l} + \cdots\right\} , \quad (26)$$

$$v_0 \approx v_a \left[1 - \frac{3}{5}\left[\frac{\rho_a}{\rho_{\mathrm{av}}} + \frac{l}{v_a}\frac{d}{dt}\ln(p_a)\right]\frac{s}{l} + \cdots\right] . \quad (27)$$

If, to the contrary, after an initial transient time, region 1 were to remain with uniform entropy (homoentropic flow), a solution through all of region 1, $-l < s < 0$, may be obtained easily. From Eq. (22) we get

$$\frac{p_0}{\rho_0^{5/3}} \approx \mathrm{const} = \frac{p_a}{\rho_a^{5/3}} , \quad (28)$$

and using Eq. (23)

$$\left[\frac{p_0}{p_a}\right]^{2/5} = \left[\frac{\rho_0}{\rho_a}\right]^{2/3} = \frac{T_0}{T_a} \approx 1 + \frac{s}{l} , \quad (29)$$

from which we obtain the average density $\rho_{\mathrm{av}} \approx 2\rho_a/5$. Following with this approximation we could then integrate Eq. (20) to get the velocity

$$v_0 \approx v_a + \left[v_a + \frac{dl}{dt}\right]\frac{s}{l} , \quad (30)$$

where the time derivative of the instantaneous target thickness, dl/dt, through the use of the mass flow rate at the ablation surface $\dot{m} \equiv \rho_a v_a \approx -d(\rho_{\mathrm{av}} l)/dt$, is given by

$$\frac{dl}{dt} \approx -\frac{5}{2}v_a - l\frac{d\ln\rho_a}{dt} . \quad (31)$$

Now, with Eq. (21), one could determine the corrections to the pressure through region 1:

$$\frac{5p_a}{2\rho_a}\left[\left[\frac{p_0}{p_a}\right]^{2/5} - 1\right] \approx s\left[g - \frac{dv_a}{dt}\right] - \frac{1}{2}(v_0^2 - v_a^2) - \frac{s^2}{2}\left[\frac{v_a}{l} + \frac{d\ln\rho_a}{dt}\right] , \quad (32)$$

and then one can obtain, using the fact that the pressure at the rear side of the slab is zero, the correction to the

acceleration g of the ablation surface obtained in Eq. (20):

$$g \approx \frac{p_a}{\rho_{av} l} - \frac{3}{2}\frac{dv_a}{dt} - \frac{31}{8}\frac{v_a^2}{l} - \frac{l}{2}\left[\frac{d^2 \ln \rho_a}{dt^2} + \left[\frac{d \ln \rho_a}{dt}\right]^2\right] - \frac{11}{2} v_a \frac{d \ln \rho_a}{dt} . \tag{33}$$

Notice that since $d/dt \sim v_a/l$, Eq. (33) shows that $g = (p_a/\rho_{av} l)[1 + O(M_a^2)] \approx p_a/\rho_{av} l$.

2. Perturbed solution

The perturbations in region 1 may be easily and consistently treated if their wavelengths are smaller than the thickness of such a region. The entropy equation (A5) may be therefore integrated, neglecting heat conduction, which yields the entropy mode

$$\frac{3}{2}\frac{T_1}{T_0} - \frac{\rho_1}{\rho_0} \approx \text{const} \times \exp\left[-\int \frac{\gamma}{v_0} ds\right] . \tag{34}$$

Assuming the real part of γ is positive, the constant appearing in Eq. (34) must be zero in order for the solution to be bounded ($s \to -\infty$), hence a relation between the perturbed pressure $p_1 \equiv \rho_1 T_0 + \rho_0 T_1$ and the perturbed density ρ_1 is obtained:

$$\rho_1 \approx \frac{3}{5}\frac{p_1}{p_0}\rho_0 . \tag{35}$$

Then, having in mind that we are mainly interested in wavelength perturbations smaller than the thickness of the slab, $kl > 1$, only the leading terms of the zero order solution are needed. First of all in order to determine the different modes we eliminate the inhomogeneous terms of Eqs. (A1)–(A3), writing the solution in the following way:

$$p_1 = p_{1h} + \xi \rho_0 g, \quad v'_{1x} \approx v_{1xh} - \gamma \xi + \xi \frac{dv_0}{ds}, \quad v_{1y} = v_{1yh} . \tag{36}$$

Moreover, since the compressibility effects are $O[(\gamma/kc_s)^2] \sim (kl)^{-1} \ll 1$, where $c_s \sim p_0/\rho_0$ is the sound velocity inside the slab, the resulting Eqs. (A1)–(A3) may be simplified as follows:

$$\frac{d}{ds}(\rho_0 v_{1xh}) + ik\rho_0 v_{1yh} \approx -\gamma \frac{3}{5}\frac{\rho_0}{p_0} p_{1h} , \tag{37}$$

$$\rho_0 \left[\gamma + v_0 \frac{d}{ds}\right] v_{1xh} \approx -\frac{dp_{1h}}{ds} + \frac{3}{5}\frac{p_{1h}}{p_0}\rho_0 g , \tag{38}$$

$$\rho_0 \left[\gamma + v_0 \frac{d}{ds}\right] i v_{1yh} \approx k p_{1h} . \tag{39}$$

Then, after some algebra we get

$$\left[\frac{d^2}{ds^2} - k^2\right] p_{1h} \approx \frac{3}{5}\rho_0 g \frac{d}{ds}\frac{p_{1h}}{p_0} + \gamma^2 \frac{3}{5}\frac{\rho_0}{p_0} p_{1h} , \tag{40}$$

whose solution corresponds to two modes of the form

$$p_{1h\pm} \approx A_\pm \exp(r_\pm s) , \tag{41}$$

$$i\rho_0 v_{1yh\pm} \approx -\frac{\rho_0 v_{1xh\pm}}{r_\pm/k - 3g\rho_0/5kp_0} \approx \frac{p_{1h\pm}}{(r_\pm/k)(\gamma/r_\pm + v_0)} .$$

$$r_\pm \approx \pm k + \frac{3k\rho_0}{10p_0}\left[\frac{g}{k} \pm \left[\frac{\gamma}{k}\right]^2\right] . \tag{42}$$

Finally we have the vorticity mode

$$p_{1h} \approx 0, \quad v_{1xh} \approx \frac{kv_0}{\gamma} i v_{1yh} \approx B_- \exp\left[-\gamma \int \frac{ds}{v_0}\right] . \tag{43}$$

In order for the solution to remain bounded ($s \to -\infty$), we must have $A_- = B_- \equiv 0$.

Let C_1 and C_2 be the perturbed mass flow rate and momentum flux in the x direction, respectively, at $s = 0^-$ (with respect to the moving perturbed ablation surface); then using Eqs. (36), (41), and (42) we have

$$C_1 \equiv (\rho_0 v'_{1x} + \rho_1 v_0)|_{s=0^-} \approx -\gamma \xi \rho_a - \frac{k}{\gamma} A_+ \left\{1 - \frac{kv_a}{\gamma} - \frac{3\rho_a}{10p_a}\left[\frac{g}{k} - \left[\frac{\gamma}{k}\right]^2\right]\right\} , \tag{44}$$

$$C_2 \equiv (p_1 + 2\rho_0 v_0 v'_{1x} + \rho_1 v_0^2)|_{s=0^-} \approx A_+ + \xi \rho_a g + 2v_a C_1 , \tag{45}$$

$$v_{1y}\Big|_{s=0^-} \approx i\left[\frac{C_1}{\rho_a} + \gamma\xi\right]\left[1 + \frac{3g\rho_a}{10kp_a} - \frac{3\rho_a}{10p_a}\left[\frac{\gamma}{k}\right]^2\right] , \tag{46}$$

$$\rho_1|_{s=0^-} \approx \frac{3\rho_a}{5p_a}(C_2 - 2v_a C_1) \sim (k\xi)\rho_a \left[\frac{\gamma}{kc_s}\right]^2 \ll (k\xi)\rho_a , \tag{47}$$

Eliminating the A_+ constant from Eqs. (44) and (45) we get (neglecting kv_a^2/g terms) the following relation between C_1, C_2, and the ablation surface deformation ξ:

$$C_2 \approx \xi \rho_a g + C_1 v_a \left\{1 - \frac{\gamma}{kv_a}\left[1 + \frac{3\rho_a g}{10kp_a} - \frac{3\rho_a}{10p_a}\left[\frac{\gamma}{k}\right]^2\right]\right\} - \gamma \xi \rho_a v_a \left\{1 + \frac{\gamma}{kv_a}\left[1 + \frac{3\rho_a g}{10kp_a} - \frac{3\rho_a}{10p_a}\left[\frac{\gamma}{k}\right]^2\right]\right\} . \tag{48}$$

This last expression is similar to the one obtained by Bodner [3] except in two aspects. One of them is due to the fact that we are using here a different formalism, which produces the ξ terms in Eq. (48); the other one comes from the retained compressibility effects (the factors proportional to $\rho_a/p_a \sim c_s^{-2}$). Such small correction terms were not taken into account by the author in Ref. [15] for simplicity in the exposition.

B. Analysis of region 2 (the thin ablation layer)

This region is very thin and its characteristic thickness is of the order of Δ, the one that depends [see Eq. (5)] fundamentally on the temperature of the target evaluated where the density reaches a maximum $T_a = p_a/\rho_a$. To study such a region it is enough to consider distances $s \sim \Delta$; then the equations are simplified to a large extent since any other characteristic length involved in the problem, k^{-1}, l, L, is much greater. The asymptotic solutions obtained in this layer have to match, taking the appropriate limits $s/\Delta \to \pm\infty$ (but keeping both ks and $\gamma\Delta/v_a$ small) to the solutions of regions 1 and 3.

1. *Unperturbed solution*

Mass and momentum conservation yield

$$\rho_0 v_0 \approx \dot{m}, \quad \rho_0 T_0 \approx p_a \tag{49}$$

and to obtain the last of Eq. (49) we have neglected the dynamical pressure $\rho_0 v_0^2 \sim M_a^2 p_a$ and the gravity effect $\sim \rho_a g \Delta \sim p_a \Delta/l$. On the other hand the simplified energy equation, neglecting the same effects, is written as

$$\frac{d}{ds}\left[\frac{5}{2}\rho_0 v_0 T_0 - \bar{K}\frac{T_0^n}{p_0^\mu}\frac{dT_0}{ds}\right] \approx 0 . \tag{50}$$

Now, integrating Eq. (50) once, and imposing the matching condition to region 1 ($s/\Delta \to -\infty$) where $T_0 \approx T_a$ and heat flux vanishes, we get

$$\frac{5}{2}\rho_0 v_0 T_0 - \bar{K}\frac{T_0^n}{p_a^\mu}\frac{dT_0}{ds} \approx \frac{5}{2}\rho_a v_a T_a . \tag{51}$$

For specified values of n Eq. (51) may be integrated once more, for instance, in the case of laser fusion ($n = 5/2$, $\mu \equiv 0$) we obtain

$$\frac{5}{2}\frac{s}{\Delta} + \text{const} = \frac{2}{5}\left[\frac{T_0}{T_a}\right]^{5/2} + \frac{2}{3}\left[\frac{T_0}{T_a}\right]^{3/2} + 2\left[\frac{T_0}{T_a}\right]^{1/2} + \ln\left[\frac{(T_0/T_a)^{1/2}-1}{(T_0/T_a)^{1/2}+1}\right] , \tag{52}$$

and the value of the constant appearing above depends on the choice of the origin, which is obviously arbitrary. The behavior of the solution of Eq. (51) for large $|s/\Delta|$ and arbitrary n value is

$$T_0 \approx \begin{cases} T_a\left[\left[\frac{5n}{2}\frac{s}{\Delta}\right]^{1/n} - \frac{1}{n-1} + \cdots\right] \approx \left[\frac{5p_a^\mu \dot{m}}{2\bar{K}}s\right]^{1/n} + \cdots, & s/\Delta \to +\infty , \\ T_a\left[1 + \exp\left[\frac{5}{2}\frac{s}{\Delta}\right] + \cdots\right], & s/\Delta \to -\infty . \end{cases} \tag{53}$$

Note as in the first of the above expressions ($s/\Delta \to +\infty$) the characteristic scale length Δ and scale temperature T_a have disappeared.

2. *Perturbed solution*

Perturbed quantities can be obtained in a simple way through mass, momentum, and energy conservation, since $k\Delta \ll 1$ and $\gamma\Delta/v_a \ll 1$ and therefore transverse and time derivatives are negligible. It is straightforward from Eqs. (A1) and (A2) of the Appendix to obtain the solution matching (at $s/\Delta \to -\infty$ but keeping $|ks| \ll 1$) to region 1:

$$\rho_1 v_0 + \rho_0 v'_{1x} \approx \text{const} = C_1 , \tag{54}$$

$$\rho_1 T_0 + \rho_0 T_1 + 2\rho_0 v_0 v'_{1x} + \rho_1 v_0^2 \approx \text{const} = C_2 . \tag{55}$$

Integrating Eq. (A3) through the use of $d(\rho_0 T_0)/ds \approx -\rho_0 v_0 d v_0/ds$ and matching to region 1 one obtains

$$i v_{1y} - k\xi v_0 \approx \text{const} = -\left[\frac{C_1}{\rho_a} + \gamma\xi\right]\left[1 + \frac{3g\rho_a}{10kp_a} - \frac{3\rho_a}{10p_a}\left[\frac{\gamma}{k}\right]^2\right] - k\xi v_a , \tag{56}$$

and finally, integrating once the energy equation, Eq. (A4), and matching to region 1 the leading terms become

$$\rho_0 v_0 \frac{5}{2}T_1 + \left[C_1 + \mu\frac{C_2}{p_a}\dot{m}\right]\frac{5}{2}T_0 - \frac{d}{ds}\left[\frac{\bar{K}T_0^n}{p_a^\mu}T_1\right] \approx \text{const} \approx T_a\left[\frac{5}{2}\left[C_1 + \mu\frac{C_2}{p_a}\dot{m}\right] + \frac{\dot{m}}{p_a}C_2\right] . \tag{57}$$

Integrating once more gives us

$$T_1 \approx \left[\frac{T_a}{T_0}\right]^n (T_0 - T_a)\left[C_3 + \frac{5}{2}\left[\frac{C_1}{\dot{m}} + \mu\frac{C_2}{p_a}\right]\frac{s}{\Delta}\right] + \frac{2C_2}{5p_a}\left[1 - \frac{5n}{2}\left[\frac{T_a}{T_0}\right]^n (T_0 - T_a)\int \frac{1}{T_0(s)}\frac{ds}{\Delta}\right] , \tag{58}$$

with C_3 being, as in Eq. (52), an arbitrary constant depending on the choice of the origin.

C. Analysis of region 3 (the near hot plasma corona)

The unperturbed solution that is emerging from region 2 ($s/\Delta \to +\infty$) shows us the characteristic feature of the fact that there exists a free scale length zone $\Delta \ll s \ll L$ in region 3. Then, to analyze this region ($s>0$), because we are interested in the wavelength perturbations $kl \sim (kL)^{1/n} \gg 1$, only a layer of thickness $s \sim k^{-1} \ll L$ needs to be considered; let then $\eta \equiv ks$ be the normalized space variable in this layer and define the small parameter $\delta \equiv (kL)^{-1/n}$. The discussion presented in a previous section about the scale of the variables in such a layer, ν_*, ρ_*, and T_* [see Eq. (11)] suggests normalizing the density, temperature, and velocity with those values, $\rho_{\rm cor}/\delta$, $T_{\rm cor}\delta$, and $\nu_{\rm cor}\delta$, respectively.

1. Unperturbed solution

In general there is no quasisteady solution throughout region 3 except in a restricted zone ($\sim k^{-1}$) next to the ablation surface. Let ζ_0, θ_0, and v_0 be the normalized density, temperature, and velocity

$$\rho_0 = \frac{\rho_{\rm cor}}{\delta}\zeta_0, \quad T_0 = \delta T_{\rm cor}\theta_0, \quad \nu_0 = \delta \nu_{\rm cor} v_0 . \tag{59}$$

The continuity, momentum, and energy equations give us

$$\frac{d(\zeta_0 v_0)}{d\eta} = 0 , \tag{60}$$

$$\delta \zeta_0 v_0 \frac{dv_0}{d\eta} = -\frac{d(\zeta_0\theta_0)}{d\eta} + \frac{\rho_a}{\rho_{\rm av}}\frac{(kL)^{1/n}}{kl} M_a^2 \zeta_0 , \tag{61}$$

$$\frac{d}{d\eta}\left[\zeta_0 v_0 \left[\frac{5}{2}\theta_0 + \frac{1}{2}\delta v_0^2\right] - \frac{5n}{2}\frac{\theta_0^{n-\mu}}{\zeta_0^{\mu}}\frac{d\theta_0}{d\eta}\right] = \frac{\rho_a}{\rho_{\rm av}}\frac{(kL)^{1/n}}{kl} M_a^2 \zeta_0 v_0 , \tag{62}$$

which can be integrated through an asymptotic expansion in the parameter δ to obtain the solution matching at $\eta \to 0^+$ to the leading term of the emerging solution of region 2 [see the first of the Eqs. (53)]:

$$\zeta_0 \approx \eta^{-1/n} - \frac{[6+5(n-\mu)]}{5(1+n)}\delta + \cdots , \tag{63}$$

$$v_0 \approx \eta^{1/n} + \frac{[6+5(n-\mu)]}{5(n+1)}\eta^{2/n}\delta + \cdots , \tag{64}$$

$$\theta_0 \approx \eta^{1/n} + \frac{(1-5\mu)}{5(1+n)}\eta^{2/n}\delta + \cdots , \tag{65}$$

having neglected $O(\delta^2)$ terms and of course $O(M_a^2)$. Notice that the small parameter δ is of the order of magnitude of the characteristic Mach number squared in such a layer $\sim \nu_*^2/T_*$, which is assumed much larger than M_a^2. On the other hand, the assumption of quasisteady flow is well satisfied since $\partial/\partial t \sim \nu_a/l \ll \nu_0 \partial/\partial s \sim k\nu_{\rm cor}/(kL)^{1/n}$.

2. Perturbed solution

The asymptotic analysis is complex and requires a power expansion with respect to two assumed small parameters: one of them is δ, and the other one is $\varepsilon \equiv \gamma/(k\nu_{\rm cor}\delta)$, which takes into account the effect of the time derivative of the perturbed solution ($\sim\gamma$) versus convective derivatives ($\sim k\nu^* \sim k\nu_{\rm cor}\delta$). Then, if one is interested in the wavelength perturbations $kl \sim (kL)^{1/n}$ we can derive the following ordering:

$$\varepsilon \equiv \frac{\gamma}{k\nu_{\rm cor}\delta} = \frac{\gamma}{k\nu_a} M_a^2 (kL)^{1/n} \sim \sqrt{k\nu_a^2/g} \sim \sqrt{klM_a^2} \ll 1 . \tag{66}$$

Notice that from Eqs. (9) and (66) we also have $\varepsilon \sim [(kL)^{1/n} M_a^2]^{1/2} \equiv (M_a^2/\delta)^{1/2} \sim [(k\Delta)^{1/n}]^{1/2}$. On the other hand, Eq. (59) shows us that the small parameter ε will enter in the unperturbed solution expansion in second order through the matching condition with region 2, for instance, $\theta_0(\eta \to 0^+) \sim T_a M_a^2/\delta \sim \varepsilon^2$. We then normalize as follows, taking into account the size scale of the perturbations and the fact that they must be proportional to the deformation ξ of the ablation surface:

$$\rho_1 T_0 + \rho_0 T_1 = \delta k \xi p_a P , \tag{67}$$

$$\rho_0 v_{1x}' + \rho_1 v_0 = k\xi \dot{m} F , \tag{68}$$

$$\nu_{1y} = \delta k \xi \nu_{\rm cor} V , \tag{69}$$

$$T_1 = \delta k \xi T_{\rm cor} \Theta , \tag{70}$$

and let the row vector $W = \{F, P, V, \eta\Theta, d(\eta\Theta)/d\eta\}$. We write the fifth order system Eqs. (A1)–(A4) in vector form using Eqs. (63)–(65) and (67)–(70):

$$\frac{dW^T}{d\eta} = AW^T + B^T , \tag{71}$$

where A is a matrix and B is a row vector coming from the inhomogeneous terms involving ξ; both depend on η, ε, and δ.

In order to connect regions 2 and 3 the solution in region 3 at $\eta \to 0^+$ must be matched to the solution emerging from region 2 at $s/\Delta \to +\infty$ (with $ks \ll 1$), which only contains in such a limit the two unknown constants C_1 and C_2. Explicitly the perturbed mass flow rate and momentum flux in region 3 must be equal to C_1 and C_2 at $\eta \to 0^+$, respectively, while both the perturbed velocity ν_{1y} and temperature in region 3 must match, at $\eta \to 0^+$, the behavior of the emerging solution from region 2, Eqs. (56) and (58) at $s/\Delta \to +\infty$, which we reproduce below, up to first order in δ and ε in the scale of variables of region 3:

$$\left.\frac{i\nu_{1y}}{(k\xi)\delta\nu_{\rm cor}}\right|_{s/\Delta \to +\infty} \approx \eta^{1/n} - \varepsilon + \frac{[6+5(n-\mu)]}{5(n+1)}\eta^{2/n}\delta + \cdots , \tag{72}$$

TABLE I. Coefficients f_1, f_2 for several values of n.

n	f_1	f_2
2.5	1.026 648	−0.520 516
4.0	1.010 964	−0.326 075
4.5	1.008 913	−0.290 704
5.0	1.007 394	−0.262 418
5.5	1.006 235	−0.239 249
6.0	1.005 331	−0.219 904
6.5	1.004 611	−0.203 496
7.0	1.004 028	−0.189 396
7.5	1.003 550	−0.177 145
8.0	1.003 153	−0.166 397

$$\left.\frac{T_1}{(k\xi)\delta T_{\rm cor}}\right|_{s/\Delta\to+\infty}\approx\frac{\eta^{1/n}}{n}\left[\frac{C_1}{\dot{m}k\xi}+\mu\frac{C_2}{p_a k\xi}\right]+\cdots . \tag{73}$$

Then, the solution in region 3, after using the boundary conditions at $\eta\approx 0^+$, will linearly depend on the constants C_1 and C_2. Moreover, it has two unbounded modes as $\eta\to+\infty$ [8], hence the condition that the solution must be bounded will determine C_1 and C_2. In order to numerically determine those constants we expand them, for instance, $C_1/(\dot{m}k\xi)\approx f_1+f_2\varepsilon+f_3\delta+\cdots$, as follows:

$$\frac{C_1}{\dot{m}k\xi}\equiv f\approx f_1+f_2\frac{\gamma}{k\nu_a}M_a^2(kL)^{1/n}+f_3(kL)^{-1/n}+\cdots , \tag{74}$$

$$\frac{C_2}{\delta p_a k\xi}\equiv q\approx q_1+q_2\frac{\gamma}{k\nu_a}M_a^2(kL)^{1/n}+q_3(kL)^{-1/n}+\cdots , \tag{75}$$

where f_j and q_j represent eigenvalues to be determined. We also expand $W=w_1+\varepsilon w_2+\delta w_3+\cdots$, $A=a_1+\varepsilon a_2+\delta a_3+\cdots$, $B=b_1+\varepsilon b_2+\delta b_3+\cdots$, and Eq. (71) gives us the following heirarchy of a fifth order system of linear differential equations with variable coefficients: in order unity,

$$\frac{dw_1^T}{d\eta}=a_1w_1^T+b_1^T ; \tag{76}$$

in order ε,

$$\frac{dw_2^T}{d\eta}=a_1w_2^T+b_2^T+a_2w_1^T ; \tag{77}$$

in order δ,

$$\frac{dw_3^T}{d\eta}=a_1w_3^T+b_3^T+a_3w_1^T , \tag{78}$$

where a_1,a_2,a_3 and b_1,b_2,b_3 are matrix and row vector functions, respectively, which only depend on η, n, and μ and are given in Appendix B.

The eigenvalues f_j, q_j are determined in each order imposing the vanishing of the perturbed solution as $\eta\to+\infty$. The homogeneous system corresponding to each equation of the hierarchy of Eqs. (76)–(78), presents two unbounded modes. To know analytically the behavior of such modes as $\eta\to+\infty$ is crucial in order to determine correctly the numerical values of f_j,q_j, mainly in this case since both modes explode as $\exp(\eta)$ [for instance, $\eta\Theta_j\sim\eta^{(3\pm\sqrt{5})/(4n)}\exp(\eta)$] [24]; this makes the numerical determination of f_j,q_j troublesome. Notice that this last point has been always unsatisfactorily treated in the past [7–9], through an incorrect determination of the behavior of the solution for large η. In Appendix D the method used for the determination of the asymptotic behavior of the solution is shown. We give in Tables I–IV the f_j,q_j for different values of n and μ.

III. THE DISPERSION RELATION

Once C_1 and C_2 have been determined (or equivalently f_j, q_j), Eq. (48) relating both constants will give us the dispersion relation

$$(1+\alpha)\gamma^2+k\nu_a[1+f(1+\alpha)]\gamma-kg\left[1-\frac{\rho_{\rm av}}{\rho_a}\frac{kl}{(kL)^{1/n}}q\right]=0 , \tag{79}$$

where

TABLE II. Coefficient f_3 for several values of n and μ (notice that f_1, f_2 are independent on μ).

	f_3					
n/μ	0	1	1.25	1.5	1.75	2
2.5	−0.011 85					
4		0.220 163	0.306 708	0.393 282	0.479 851	0.566 419
4.5		0.223 584	0.312 920	0.402 238	0.491 554	0.580 890
5.0		0.226 983	0.318 674	0.410 396	0.502 150	0.593 901
5.5		0.230 141	0.323 987	0.417 803	0.511 650	0.605 521
6.0		0.233 206	0.328 900	0.424 580	0.520 248	0.615 932
6.5		0.236 010	0.333 392	0.430 688	0.528 035	0.625 385
7.0		0.238 680	0.337 506	0.436 256	0.535 065	0.633 928
7.5		0.241 149	0.341 274	0.441 399	0.541 589	0.641 689
8		0.243 374	0.344 758	0.446 052	0.547 464	0.648 755

$$\alpha \equiv \frac{3}{10}\frac{\rho_a}{p_a}\left[\frac{g}{k}-\left[\frac{\gamma}{k}\right]^2\right] \approx \frac{3}{10}\frac{q}{(kL)^{1/n}} . \quad (80)$$

To obtain Eq. (79) terms like $kv_a^2/g \sim \varepsilon^2$ have been neglected and, on the other hand, the approximation used in Eq. (80) lies in the fact that we are taking the leading term for γ in Eq. (79). The retaining up to first order in δ and ε, the unstable root is

$$\gamma \approx \left\{kg\left[1-\frac{\rho_{\rm av}}{\rho_a}\frac{kl}{(kL)^{1/n}}\left[q_1+\frac{q_3-(3/10)q_1^2}{(kL)^{1/n}}+\frac{3}{10}\frac{\rho_a}{\rho_{\rm av}}\frac{q_1}{kl}\right]\right]\right\}^{1/2} - kv_a(1+f_1+q_2)/2 . \quad (81)$$

A. Stabilization mechanism

It is clear that Eqs. (74) and (75) point out the mechanism of stabilization. On the one hand we have the so-called "fire polishing effect," as Eq. (74) suggests; the crest of the rippled ablation surface coming into the corona is evaporating more quickly than the valley, enhancing this effect by heat conduction (terms involving kL). On the other hand, Eq. (75) shows the dominant stabilization effect, the overpressure generated on the crest of the corrugated ablation surface due to heat conduction; this effect damps and could stop its growth.

We point out that the factor multiplying kv_a above (the so-called ablative stabilization), $(1+f_1+q_2)/2$, takes a value of approximately 2 for the entire range of interest in n and μ values (becoming a general feature of the ablatively accelerated targets), with q_2, the term coming from the momentum flux contribution through the ablation front, being the largest. Strictly, in the asymptotic limit $M_a \to 0$, the growth is stabilized (neglecting kv_a) because the square root term in Eq. (81) vanishes for a cutoff wave number

$$k_c l \approx \left[\frac{\rho_a}{q_1\rho_{\rm av}}\right]^{n/(n-1)}\left[\frac{L}{l}\right]^{1/(n-1)} \times\left[1-\frac{q_3}{q_1}\left[\frac{q_1\rho_{\rm av}}{\rho_a}\right]^{1/(n-1)}\left[\frac{l}{L}\right]^{1/n(n-1)}\right] , \quad (82)$$

and the condition $k_c\Delta \ll 1$ in order for the model to be consistent is explained as

$$\frac{\Delta}{l} \ll \left[\frac{5n}{2}\right]^{1/n} q_1\frac{\rho_{\rm av}}{\rho_a}M_a^2 . \quad (83)$$

For wave numbers $k > k_c$, the modes become oscillatory, similarly to the effect produced by surface tension in liquids. The main stabilizing effect is due to heat conduction, which causes the momentum flux to increase on the crests of the rippled ablation front and decrease in the valley, damping the growth of the unstable ablation front and being able to stop it. On the other hand, the kv_a term in Eq. (77) or the so-called ablative stabilization effect also helps to damp the growth. Both stabilizing effects would be increased substantially by means of reduced values of L and the peak density ρ_a (for $\dot{m}$ fixed), respectively. Finally, we emphasize that Eq. (81) has been rigorously derived without any assumption regarding the behavior of the far away plasma corona or laser energy deposition region, which affects the determination of L.

TABLE III. Coefficients q_1, q_2, q_4, q_5, for several values of n.

n	q_1	q_2	q_4	q_5
2.5	0.667 5622	2.07611	3.74950	−0.105 2360
4.0	0.760 6308	2.04015	3.83162	−0.025 3521
4.5	0.781 1391	2.03351	3.84453	−0.018 6037
5.0	0.798 4274	2.02835	3.85526	−0.014 2478
5.5	0.813 1950	2.02429	3.86491	−0.011 2696
6.0	0.825 9536	2.02103	3.87373	−0.009 1417
6.5	0.837 0855	2.01837	3.88344	−0.007 5676
7.0	0.846 8823	2.01619	3.89055	−0.006 3697
7.5	0.855 5701	2.01437	3.89671	−0.005 4366
8.0	0.863 3266	2.01284	3.90204	−0.004 6954

B. Theoretical determination of the coronal characteristic length L

Throughout the problem, L has been assumed to be a known parameter. In fact L is an eigenvalue of the unperturbed problem, which is in general determined for a given target and radiation conditions. L is defined [see Eq. (6)] by means of p_a and $\dot{m}$ values, which can be derived from either one-dimensional numerical simulations, experiments, or analytical models. For instance, some known scaling laws for planar analytical models in laser fusion ($p_a \sim I_L^{2/3}\lambda_L^{-2/3}$, $\dot{m} \sim I_L^{1/3}\lambda_L^{-2/3}$) [25] leads to $L \sim I_L^{4/3}\lambda_L^{14/3}$, where I_L is laser intensity and λ_L is laser wavelength. On the other hand, spherical and planar analytical models [7,8], if energy is absorbed in the supersonic region of the corona, lead to L/l, depending basically on the ratio of the sonic, ρ_s, to the ablation, ρ_a, densities (or equivalently M_a) and the aspect ratio r_a/l (if spherical), with r_a the ablation radius. In fact, the isothermal sonic point of the corona where $v_0^2 = p_0/\rho_0$ represents a singular point of the system of the hydrodynamic equations, and the condition for a continuous transonic solution to exist leads to a universal relation between ablation pressure and mass flow rate (such a relation was implicitly used in the results presented in Ref. [7] and some numerical values were also given in Ref. [8]). One can obtain L explicitly in a closed form assum-

TABLE IV. Coefficient q_3 for several values of n and μ (notice that q_1, q_2 are independent on μ).

	q_3				
n/μ	0	1	1.25	1.5	1.75	2
2.5	0.606 840					
4		1.185 638	1.305 321	1.425 067	1.544 803	1.664 539
4.5		1.242 812	1.370 454	1.498 056	1.625 653	1.753 293
5.0		1.293 756	1.428 370	1.563 054	1.697 811	1.832 560
5.5		1.339 074	1.480 161	1.621 180	1.762 270	1.903 413
6.0		1.379 938	1.526 738	1.673 505	1.820 244	1.967 022
6.5		1.416 641	1.568 708	1.720 585	1.872 575	2.024 573
7.0		1.449 994	1.606 700	1.763 237	1.919 907	2.076 694
7.5		1.480 283	1.641 217	1.802 152	1.963 232	2.124 110
8		1.507 769	1.672 757	1.837 551	2.002 602	2.167 387

ing $M_a^2 \ll 1$ and having in mind that it is a roughly approximated description for the flow not too far from the pellet, say, at some small fraction of r_a.

1. *Absorption at the supersonic region*

Let us consider as in Refs. [7,8] the mass, momentum, and energy conservation equations in spherical geometry:

$$r^2\rho_0 v_0 = \text{const} \equiv r_a^2 \dot{m} \ , \tag{84}$$

$$\rho_0 v_0 \frac{dv_0}{dr} = -\frac{d(\rho_0 T_0)}{dr} + \rho_0 g \ ,$$

$$r^2\rho_0 v_0 \left[\frac{5}{2} T_0 + \frac{1}{2} v_0^2 - g(r - r_a) \right] - r^2 \frac{\bar{K} T_0^{n-\mu}}{\rho_0^{\mu}} \frac{dT_0}{dr} \approx 0 \ , \tag{85}$$

where r is the radial coordinate and the gravity g has been introduced [7,8] to take into account roughly the effect of the acceleration of the ablation surface. We then normalize the variable in the following way:

$$N = \rho_0/\rho_{\text{cor}}, \quad u = v_0/v_{\text{cor}} \ ,$$
$$Z = T_0/T_{\text{cor}}, \quad X = r/r_a \tag{86}$$

and after eliminating the density we get the following two equations:

$$\frac{1}{2}\left[1 - \frac{Z}{u^2}\right]\frac{du^2}{dX} = \frac{2Z}{X} - \frac{dZ}{dX} + \hat{g} \ , \tag{87}$$

$$\frac{5}{2}Z + \frac{1}{2}u^2 - \hat{g}(X-1) = \frac{5n}{2}\hat{L} X^{2(1+\mu)} u^{\mu} Z^{n+1-\mu} \frac{dZ}{dX} \ , \tag{88}$$

where

$$\hat{g} \equiv M_a^2 \frac{\rho_a}{\rho_{\text{av}}} \frac{r_a}{l} \ ,$$

$$\hat{L} \equiv \frac{L}{r_a} \equiv \frac{1}{r_a}\left[\frac{p_a}{\dot{m}}\right]^{2n} \frac{2\bar{K}}{5n\dot{m}p_a^{\mu}} \ . \tag{89}$$

The following boundary conditions are imposed in order to solve Eqs. (87) and (88) in $X > 1$ and to obtain the eigenvalue $\hat{L}$ for each value of the parameter $\hat{g}$:

$$Z|_{X\to 1^+} \approx 0, \quad \left.\frac{Z}{u}\right|_{X\to 1^+} \approx 1 \ , \tag{90}$$

$$\left[\frac{2Z}{X} + \hat{g} - \frac{3Z - \hat{g}(X-1)}{\hat{L}X^{2(1+\mu)}Z^{n+1-\mu/2}}\right]\Bigg|_{X=X_s} = 0 \ ,$$
$$u^2|_{X=X_s} = Z|_{X=X_s} \ , \tag{91}$$

where X_s is the sonic point coordinate. The first of the boundary conditions (90) comes from the fact that $Z(X\to 1^+) \sim T_a/T_{\text{cor}} \approx 0$, while the second is expressing the fact that in normalized variables the pressure as $X \to 1^+$ is p_a. On the other hand, the boundary condition (91), corresponding to the vanishing of the right hand side of Eq. (87) at the sonic point, is the condition for a continuous transonic solution to exist.

Once the function $\hat{L}(\hat{g})$ is obtained, similar expressions also may be derived for the ratios $\rho_s/(\rho_a M_a^2) \equiv N_s(\hat{g})$,

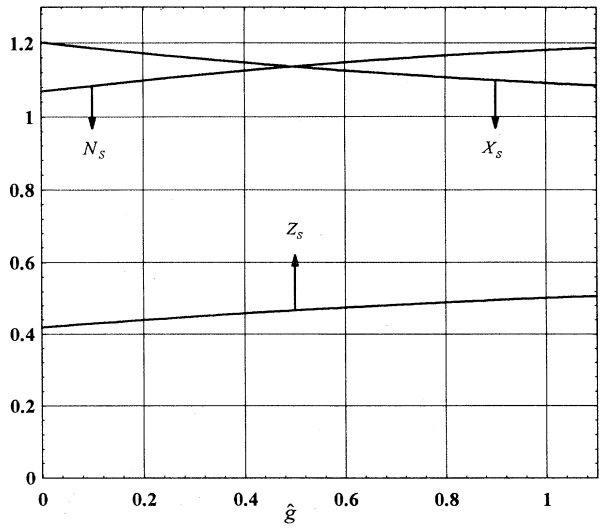

FIG. 2. Dimensionless normalized density N_S, temperature Z_S and sonic radius X_S, in the case of electronic heat conduction ($n = \frac{5}{2}$, $\mu = 0$), vs the normalized aspect ratio $\hat{g} \equiv M_a^2(\rho_a/\rho_{\text{av}})r_a/l$.

$M_a^2 T_{0S}/T_a \equiv Z_S(\hat{g})$, and the sonic ($r_s$) to ablation radius ratio $r_s/r_a \equiv X_s(\hat{g})$ [all this on the basis of the approximation, as in Refs. [7,8], that in fact the ratio $(r_s - r_a)/r_a$ is numerically small]. In Fig. 2 we give $X_S(\hat{g})$, $N_S(\hat{g})$, and $Z_S(\hat{g})$ for $n=5/2$, $\mu=0$, while in Fig. 3, we show $LM_a^2\rho_a/(\rho_{\rm av} l) \equiv \Psi(\hat{g})$, so

$$L = \frac{\rho_{\rm av}}{\rho_a}\frac{l}{M_a^2}\Psi(\hat{g}) , \tag{92}$$

and hence, the cutoff wave number is

$$k_c l \approx \frac{\rho_a}{\rho_{\rm av}}\left[\frac{\Psi}{q_1 M_a^2}\right]^{1/(n-1)}\left[1-\frac{q_3}{q_1}\left[\frac{q_1\rho_{\rm av}}{\rho_a}\right]^{1/(n-1)}\left[\frac{\rho_a}{\rho_{\rm av}}\frac{M_a^2}{\Psi}\right]^{1/n(n-1)}\right] . \tag{93}$$

We also point out the following features about the behavior of the $\Psi(\hat{g})$, which is a monotonic growing function: $\Psi(\hat{g}) \sim \hat{g}$ for $\hat{g} \ll 1$ (for instance, with low aspect ratio targets) [25] and in the opposite limit, for $\hat{g} \gg 1$ (for instance, in the case of large aspect ratio targets or in the planar case) it is $\Psi(\hat{g}) \sim$ const. We summarize the results corresponding to the laser fusion case ($n=5/2$ and $\mu=0$) as follows. Low aspect ratio:

$$L \approx 1.8 r_a , \tag{94}$$

$$k_c l \approx 2.88\left[\frac{\rho_a}{\rho_{\rm av}}\frac{r_a}{l}\right]^{2/3}\left[1-0.60\left[\frac{\rho_{\rm av}}{\rho_a}\right]^{2/3}\left[\frac{l}{r_a}\right]^{4/15}\right] ; \tag{95}$$

large aspect ratio or planar case ($\Psi \approx 0.85$):

$$L \approx 0.85\frac{\rho_{\rm av}}{\rho_a}\frac{l}{M_a^2} , \tag{96}$$

$$k_c l \approx 1.17\frac{\rho_a}{\rho_{\rm av} M_a^{4/3}}\left[1-0.73\left[\frac{\rho_{\rm av}}{\rho_a}\right]^{2/3}\left[\frac{\rho_a M_a^2}{\rho_{\rm av}}\right]^{4/15}\right] . \tag{97}$$

2. *Other situations of interest*

When gravity plays an important role in the zone where the energy deposition takes place, except for those cases considered in the previous paragraph, it is not possible to get simple analytical results within the hypothesis of a quasisteady model. It may be instructive, however, to summarize some laser fusion analytical results, which were derived in the literature neglecting (thick targets) the recoiling of the target or its acceleration.

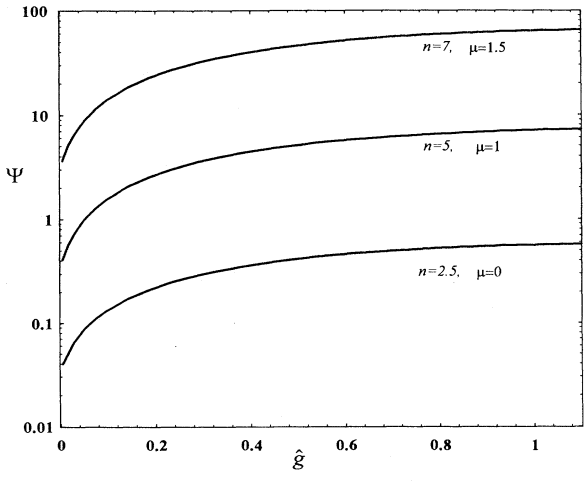

FIG. 3. Dimensionless normalized heat conduction characteristic length $\Psi \equiv LM_a^2\rho_a/(\rho_{\rm av} l)$, for several values of n and μ, vs the normalized aspect ratio $\hat{g} \equiv M_a^2(\rho_a/\rho_{\rm av})r_a/l$.

If the electron mean free path is larger than the characteristic length for temperature changes, the classical result for the electron heat flux, $\mathbf{q}_e = -\bar{K}T^{5/2}\nabla T$, yields unphysical large values. A simple but crude way to correct for this has been to saturate, or limit, the value of $\mathbf{q}_e$ in the form

$$|\mathbf{q}_e| \le \beta p_e \sqrt{T/m_e} , \tag{98}$$

where p_e is the electron pressure, m_e is the electron mass, and β is a flux limit factor, which has been discussed in detail in the literature [26]. As shown in Ref. [27], for β larger than roughly 0.04, the result $L \approx 1.8 r_a$ is unchanged, but for smaller values the flow becomes saturated before reaching the sonic point, giving in this case

$$L \approx r_a\left[\frac{5}{2\beta}\left[\frac{m_e Z_i}{m_i}\right]^{1/2}\right]^5 , \tag{99}$$

where m_i and Z_i are the ion mass and charge number, respectively. Equation (99), strictly valid for very small β, shows the inefficiency of the stabilization mechanism for strongly saturated flow.

In some simple planar and quasisteady models [28] appearing in the literature we find

$$p_a \approx \frac{2\dot{m}^2}{\rho_c} \approx 2\left[\frac{2}{5}\right]^{2/3} \rho_c^{1/3} I_L^{2/3}\,, \qquad x_c \approx \frac{4\bar{K}}{25}\left[\frac{2}{5}\right]^{4/3} \frac{I_L^{4/3}}{\rho_c^{7/3}}\,, \tag{100}$$

where ρ_c and x_c are the critical density and the distance between the ablation and the critical surfaces, respectively. Then, yielding a cutoff wave number

$$k_c l \approx 19.64 \left[\frac{\rho_a}{\rho_{\rm av}}\right]^{5/3} \left[\frac{x_c}{l}\right]^{2/3} \left[1-0.277\left[\frac{\rho_{\rm av}}{\rho_a}\right]^{2/3}\left[\frac{l}{x_c}\right]^{4/15}\right] \sim I_L^{8/9}\lambda_L^{28/9}\,, \tag{101}$$

hence, a significant reduction of the cutoff wave number occurs for short laser wavelength.

IV. COMPARISONS

A. Comparisons with numerical and theoretical results

In Fig. 4 the numerical results calculated by Takabe *et al.* [7] in the laser fusion case (solid squares), using the same normalization, for several ratios of the ablation to the sonic densities ρ_a/ρ_s, are compared with our results from Eqs. (81) and (89). For the comparisons we have used the approximation $k \approx l/r_a$, where l is the Legendre index of spherical harmonics, and the same variables as Takabe *et al.*: $G = g r_s / C_s^2$, C_s is the isothermal sound velocity at the sonic radius r_s and $\Upsilon \equiv \gamma r_s / C_S$. The results of the previous section about the spherical model have been used to perform a complete comparison, due to the absence of such complete results in Ref. [7]. In terms of our variables we have

$$G \equiv \hat{g}\frac{X_S}{Z_S}\,, \quad \frac{\rho_a}{\rho_S} \equiv \frac{1}{M_a^2 N_S}\,, \quad \Upsilon \equiv \gamma\left[\frac{r_a X_S Z_S G}{g}\right]^{1/2}. \tag{102}$$

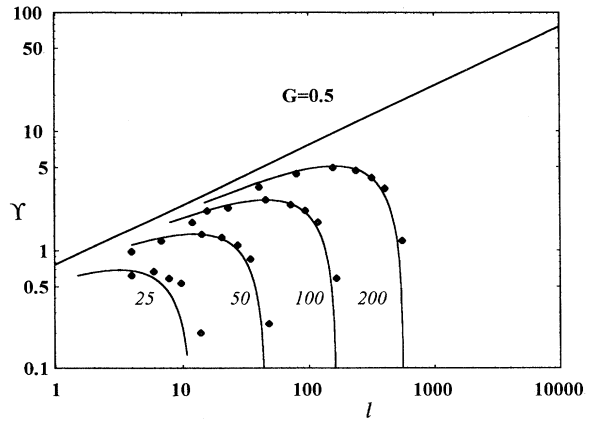

FIG. 4. Dimensionless normalized growth rate vs Legendre index for several values of ρ_a/ρ_s. Curves were obtained from Eq. (81) in the text and solid squares are points calculated by Takabe *et al.* [7]. The straight line corresponds to the classical growth $\sqrt{kg}$ in normalized units.

The results predicted by our Eq. (81) show good agreement with the results of Takabe *et al.* (solid squares). The corresponding comparisons to different values from $G=0.5$ are similar but show smaller cutoff wave numbers than those of Takabe *et al.* Their calculations in fact were performed by means of a numerical patching of the solution at different zones. Ours, however, were performed by means of rigorous asymptotic matching at different zones and hence they provide us with analytical results that show the real physical stabilization mechanism underlying the numerical Takabe *et al.* results.

Kull [8] carried out similar calculations to Takabe *et al.*, but with a better defined model, which, on the other hand, is strictly valid for much shorter wavelength perturbations; it is in fact applicable to $k\Delta \sim O(1)$ (notice that Kull's characteristic length L_1 is $\frac{2}{5}$ times our Δ characteristic length). We could compare here, Figs. 5 and 6, in the case of small Γ (and hence $k\Delta \ll 1$) the growth rate, $\sigma(\kappa,\Gamma)$, the instability boundary, $K_c(\Gamma)$, and

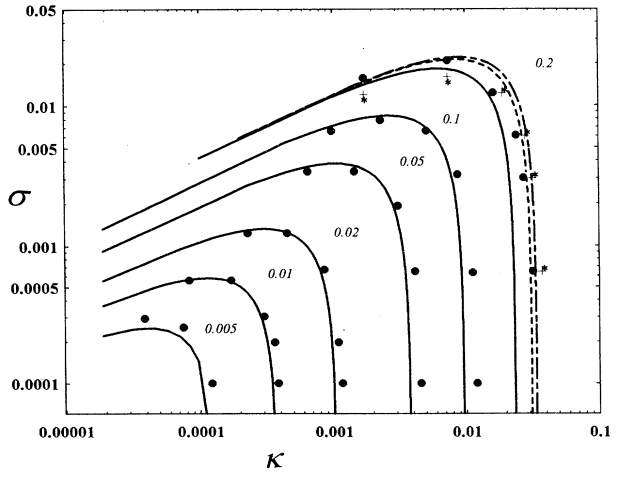

FIG. 5. Dimensionless normalized curves of instability growth rate σ, derived from Eq. (104) in the text, vs dimensionless normalized wave number κ with Γ varying between 0.005 and 0.2 (solid lines for $n=2.5$). Solid circles were obtained from the Kull [8] numerical calculations for the same values of Γ and $n=2.5$. Results derived from Eq. (104) for $\Gamma=0.2$, $n=5$ (short-dashed line) and $n=8$ (long-dashed line) are shown. The corresponding numerical calculations [8] also are shown: asterisk ($n=8$) and cross ($n=5$).

the wave number of the maximum growth, $K_m(\Gamma)$, found numerically by Kull [8] with our results. For instance, it is straightforward (see Ref. [8]) to derive in terms of the Kull variables (Γ, K, κ) the following relations:

$$\frac{L}{l}=\frac{1}{n}\frac{\rho_{\mathrm{av}}}{\rho_a}\frac{\Gamma}{M_a^{2n-2}}, \quad K\equiv\frac{\kappa}{\Gamma}=\frac{\rho_{\mathrm{av}}}{\rho_a}M_a^2 kl \ ,$$

$$\sigma=\frac{\gamma}{\sqrt{kg}}\sqrt{\kappa\Gamma} \ . \tag{103}$$

Although our analytical formula, Eq. (81), is only applicable in the case when $k\Delta \ll 1$ (and hence $\Gamma \ll 1$), our results are of interest in two respects. First, Eq. (81) contains additional information to Ref. [8], since we have, contrary to Kull, a nonisobaric model. On the other hand, Eq. (81) (for both Γ and κ small but fixed and $M_a=0$) reproduces well the numerical results of Ref. [8], shedding new light on the physical mechanism of stabilization or scale laws implicitly contained in the numerical results of Kull, at least for small Γ. Then we get from Eq. (81)

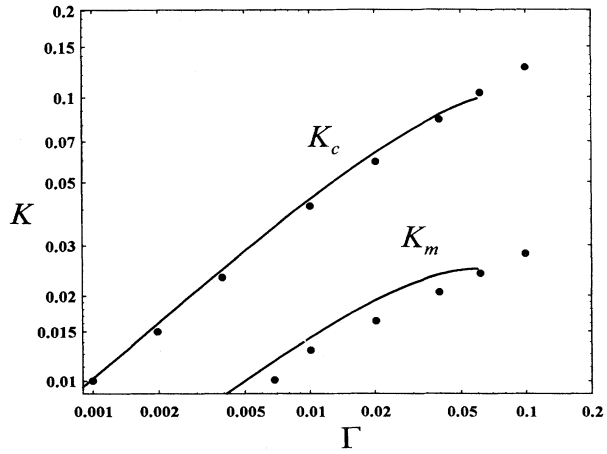

FIG. 6. Comparison of the instability boundary $K_c(\Gamma)$ and wave number $K_m(\Gamma)$ of maximum growth, derived from Eqs. (106) and (105) respectively, with the numerical (solid circles) obtained from Kull [8].

$$\sigma\approx\sqrt{\kappa\Gamma-q_1 n^{1/n}\kappa^{2-1/n}}-2\kappa \ , \tag{104}$$

and from this last equation we obtain the wave number of the maximum growth:

$$K_m\approx\left[\frac{n}{q_1(2n-1)}\right]^{n/(n-1)}\left[\frac{\Gamma}{n}\right]^{1/(n-1)}\left[1-\frac{4n}{n-1}\left[\frac{n(n-1)\Gamma^{1/(n-1)}}{q_1^{n/(n-1)}(2n-1)^{(2n-1)/(n-1)}}\right]^{1/2}\right] . \tag{105}$$

The cutoff wave number is $K_c\equiv\kappa_c/\Gamma\approx q_1^{-n/(n-1)}(\Gamma/n)^{1/(n-1)}$ as a first approximation. In order to obtain a better approximation, retaining, for instance, the κ term in Eq. (104), one must retain also the terms of order κ^2 in the radical, which means terms of second order in ε and δ. This task is very difficult, except for the case $\gamma\equiv 0$, which is the one we are interested in now. Basically, the mathematical problem is limited to consider the expansion $q\approx q_1+q_3(kL)^{-1/n}+q_4 g M_a^4(kL)^{2/n}/k\nu_a^2+q_5 M_a^2(kL)^{1/n}+\cdots$, instead of Eqs. (74) and (75) and similarly for the rest of the variables. Then we get

$$K_c\equiv\frac{\kappa_c}{\Gamma}\approx\frac{1}{q_1^{n/(n-1)}}\left[\frac{\Gamma}{n}\right]^{1/(n-1)}\left[1-\frac{n}{n-1}\frac{(q_4+q_5-f_1^2/q_1)}{(nq_1)^{1/(n-1)}}\Gamma^{1/(n-1)}\right] , \tag{106}$$

where for the case $n=\frac{5}{2}$, one has $q_4\approx 3.75$ and $q_5\approx -0.1$ (see Table III). The results of the comparisons in Figs. 5 and 6 for $n=\frac{5}{2}$ show good agreement [notice that Eqs. (104)–(106) are only valid for small Γ]. The cutoff wave number that could be derived from Fig. 5 shows somehow an error; however, a more exact determination, which is shown in Fig. 6 using Eq. (106), gives an excellent agreement with Kull's numerical results for the range of Γ values that we have used for the comparison. In Fig. 5, the curves corresponding to $n=5$ and 8 for the case $\Gamma=0.2$ are shown (the only values given in Ref. [8]) and as Kull claimed the growth rate curves show only minor variations. Our work suggests that the stabilization mechanism underlying the numerical Kull results differs from that pointed out in Ref. [8]. In fact, following Kull, let χ_a be the thermal diffusivity at the ablation front ($\sim K_a/\rho_a$), then for $\Gamma \ll 1$ stabilization is occurring at very small wave numbers, $\kappa\sim k\Delta\sim k\chi_a/\nu_a=k^2\chi_a/(k\nu_a)\ll 1$, and as shown in previous sections it is caused by the overpressure due to heat conduction $\gamma\sim\sqrt{kg}\sim[k^2(p_a-p_*)/\rho_a]^{1/2}\sim k\nu_a/(k\Delta)^{1/(2n)}\gg k\nu_a$, and hence the regime $\Gamma\ll 1$ is not stabilized by the so-called ablative convection.

In a recent paper Bychkov, Golberg, and Liberman [9] solved numerically the same equations as Kull (isobaric approximation, etc.) but with an unclear or ambiguous discussion or definition of the problem in terms of the external physical parameters. Their results [9] were given unnecessarily, by means of two parameters, which was due partly to the method of patching used in the solution of the eigenvalue problem. The results, except for differences due to the method used in the solution, should be similar to Kull's. In the same paper [9] the authors show an analytical formula for the time growth rate

in the case of very large wavelength perturbations, $kL \ll 1$, which has little physical interest, and its derivation is based in the "Landau-Darius boundary condition," which is inconsistently derived in the laser fusion case (heat conduction cannot be neglected in a consistent way). In fact, notice that from Eq. (74) one may get the prefront absolute perturbed velocity ($v_{x1}=v'_{x1}+\gamma\xi$) at the ablation surface

$$v_{x1}\approx\gamma\xi+k\xi v_a\left[f_1+f_2\frac{\gamma}{kv_a}M_a^2(kL)^{1/n}+(f_3-\tfrac{3}{5}q_1)(kL)^{-1/n}+\cdots\right]. \quad (107)$$

For the case of $kL\leq O(1)$, the previous equation cannot be applied. A similar derivation carried out by the author of the present paper is found in the literature [29] and it could be expressed as

$$v_{x1}\approx\gamma\xi+k\xi v_a\Omega\ , \quad (108)$$

where Ω is a function depending on kL and on the irradiation conditions (spherical effects, bremsstrahlung absorption, nonsteady effects, etc). In Fig. 7 we show the results for planar quasisteady geometry, neglecting inverse bremsstrahlung absorption and the deflagration regime (low laser intensity, heat conduction restricted to a thin layer next to the target [25]): the curve labeled a was plotted using the Chapman-Jouget condition [25] [one finds $\Omega\propto(kL)^{1/3}$ for $kL\ll1$]; curves labeled b and c correspond to an isothermal Mach number at the critical surface of 0.5 and 0.9, respectively (as may be seen $\Omega\approx\text{const}\neq0$ for $kL\ll1$). On the other hand in quasisteady spherical geometry and the deflagration regime too, using $k\sim l/r_a$ (l is the Legendre index) leads to $\Omega\approx-2/(3l)$. So only Eq. (107) represents a universal relation, independent of the irradiation target conditions (notice that curves a, b, and c of Fig. 7 will take asymptotically the value $f_1\approx1.03$ for $kL\gg1$). Consequently, the Landau-Darrieus boundary condition is never applicable in laser fusion except, clearly, in the case $kL=0$, for which $\gamma=\sqrt{kg}$.

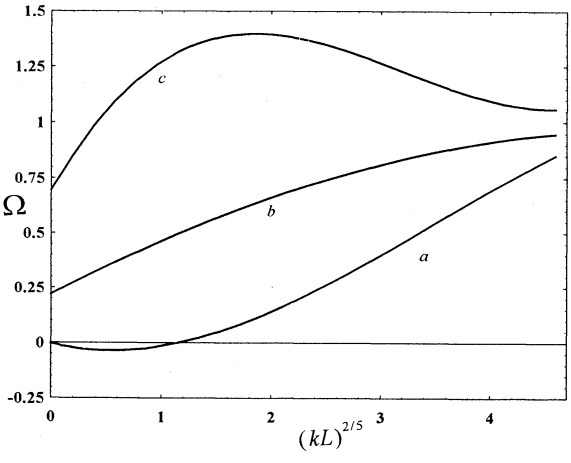

FIG. 7. The Ω function entering in the expression of the perturbed prefront velocity; see Eq. (108) in the text, vs $(kL)^{2/5}$.

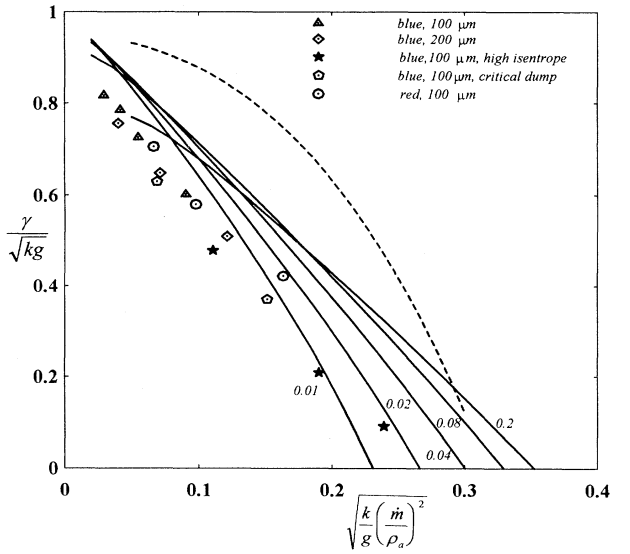

FIG. 8. Dimensionless normalized growth rate vs dimensionless normalized wave number. Curves were obtained from Eqs. (81) and (96) for different values of M_a indicated in the figure. Dashed line corresponds to the Book results [19]. Results from the numerical simulations of Gardner *et al.* [4] are also shown.

The results obtained by Book [19] are surprisingly numerically similar to ours despite the use of an incompressible model and the neglect of heat flux. In Fig. 8 we compare our results [with $L\approx0.85(\rho_{av}l)/(\rho_aM_a^2), n=\frac{5}{2}$, and $\mu=0$] with the numerical ones of Book [19]. On the other hand recently, Wouchuk and Piriz [21], using a similar model to Book's, have derived an analytical formula for the time growth rate. The authors, however, derived the formula un-self-consistently by neglecting the pressure variation in the momentum conservation along the front; in fact, the rigorously derived formula for the cutoff wave number, for instance, is $k_c=A_Tgr_D/(\phi-1)v_2^2$, instead of $k_c=A_Tgr_D/\phi v_2^2$ (see page 496 of Ref. [21]), and a similar correction needs to be made to the formula for γ. Taking into account that the dimensionless number ϕ may be very close to unity (it may be shown that $\phi=f_1\approx1.03$), this difference is very important. However, the analytical formula of the authors of that paper is in the right direction, but with an erroneous interpretation of the underlying physical stabilization mechanism. Actually, our Eq. (13) may be written in a different form, which is more transparent for this case (showing the same feature as the formula of Ref. [21]): the stabilization is occurring at $O(1)\sim kl/(kL)^{1/n}\sim kv_*^2\rho_a/(g\rho_*)$ [the asterisk denotes the variables calculated at a distance of one wavelength from the ablation surface; see Eq. (11)]. This stabilization mechanism, which underlies many of the numerical results found in the literature, is also indicated at least in the formula of

Ref. [21]. Our work indicates that it is not the ablative convection that the authors suggest. Very recently, Betti *et al.* [30] have presented a model, where the approximation of large n (the exponent entering in the conductivity coefficient) is used to obtain the cutoff wave number. The authors however did not notice that their result, at least with respect to the dominant effect, already was predicted exactly in Ref. [15]; here a more complete expression [see Eq. (106)] reproduces the same results. Our work indicates that the stabilization mechanism is not the one the authors suggest.

B. Comparison with numerical simulations and experiments

Figure 9 shows the comparison with some results of the numerical simulations (FAST2D code) reported by Gardner, Bodner, and Dahlberg [4]. L has been obtained from some of the data reported there; plastic CH targets of thickness 100 μm are exposed to blue (0.26 μm) or red (1.06 μm) laser radiation (3×10^{14} W cm^{-2}). One of them, that corresponding to critical dump (all the laser energy was deposited at critical density in the simulation), which has a value for L much smaller than the others, shows a departure from the rest, in agreement with what is predicted by Eq. (81). Such behavior cannot be only attributed to the mass ablation term of Eq. (1). Additional results of the same reference are also shown in Fig. 8.

We next compare with some LASNEX (CH targets 20 μm, 2×10^{14} W cm^{-2}, and 0.26-μm laser wavelength) and POLLUX (CH2 targets 16 μm thick, 1.5×10^{14} W cm^{-2}, and 0.53-μm laser wavelength) simulation results performed by Tabak, Munro, and Lindl and Kilkenny [4], respectively. In order to carry out the comparison the value of L has been obtained, for equivalent irradiation conditions, from the one-dimensional code MULTI (with a Planckian treatment of radiation) [31], since due to the lack of data in the corresponding references, the approximate values of $M_a\approx0.1$ and $\Psi\approx0.2$ were obtained, and hence both curves shown in Fig. 10 also were obtained in this way through Eq. (81), assuming 70% (the higher) and 40% approximately of ablated mass, respectively.

Experiments in RT instability are unusually difficult and the degree of uncertainty of measurements is important, which is crucial for a complete comparison with simulations or analytical results. In the same Fig. 10 we show the experimental results (CH2 targets 16 μm thick, 1.5×10^{14} W cm^{-2}, and 0.53-μm laser wavelength) obtained by Desselberger *et al.* [5].

Finally, for the actual conditions of a set of indirect-drive experiments [$\Delta\sim1-4$ μm is the minimum density gradient scale length $\equiv LM_a^{2n}(n+1)^{n+1}/n^n$, $kv_a^2/g<0.02$] [11], Eq. (81) leads to $\gamma\approx\sqrt{kg}-2kv_a$, which shows good agreement with the data of the experiment and the corresponding LASNEX simulation.

V. CONCLUSIONS

We have studied the Rayleigh-Taylor instability in inertial confinement fusion and we have developed a rigorous and self-consistent model that can reproduce a wide set of results found in the literature. The model presents a scaling law and stabilization mechanism and therefore sheds light on the stabilization mechanism that underlies many numerical, analytical, and simulation results. We also have compared widely with other models, some called self-consistent, indicating the similarities and differences, and we have described and solved in a clear way the puzzle of boundary conditions used in the past. We could summarize our method for solving this problem in the following way: one must use through the abla-

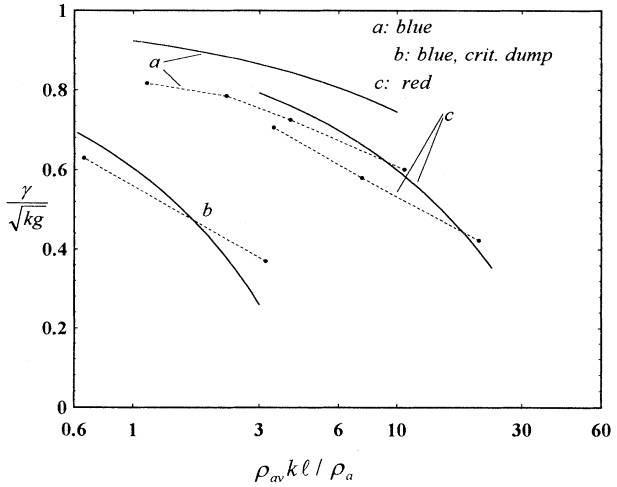

FIG. 9. Dimensionless normalized growth rate vs dimensionless normalized wave number. Curves were obtained from Eq. (81) and solid squares from the numerical simulations of Gardner, Bodner, and Dahlburg [4]. Points are joined to clarify the behavior.

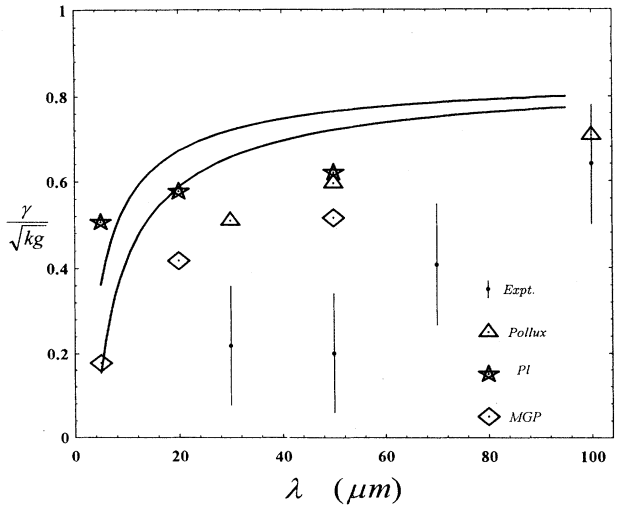

FIG. 10. Dimensionless normalized growth rate vs perturbation wavelength (μm). Curves were obtained from Eq. (81) with $M_a\approx0.1$ and $\Psi\approx0.2$ derived from MULTI [31], assuming 70% (the higher) and 40% of ablated mass, respectively. Results from simulations and experiments are also shown. The corresponding results to LASNEX with two treatments of radiation: multigroup photonic (MGP) and Planckian (PI).

tion surface the mass and momentum conservation; on the one hand, Eq. (74) expresses basically the prefront perturbed pressure as a function of the interface deformation [equivalent to the *ad hoc* Eq. (14) of Bodner in Ref. [3]], and on the other hand Eq. (75) expresses the prefront perturbed velocity as a function of the interface deformation (equivalent to the Landau-Darrieus boundary condition or an *ad hoc* modified version of it). Of course the model has limitations (for instance, targets not too thin) but it is applicable to real ICF configurations.

ACKNOWLEDGMENTS

This research was supported by the Commission Interministerial de Ciencia y de Tecnología of Spain (C92010502).

APPENDIX A

The continuity equation may be written as

$$\gamma\rho_1+\frac{d}{ds}(\rho_1 v_0+\rho_0 v'_{1x})+ik\rho_0 v_{1y}=0 , \tag{A1}$$

the momentum equation along the main flow as

$$\gamma(\rho_1 v_0+\rho_0 v'_{1x})+\frac{d}{ds}(\rho_1 T_0+\rho_0 T_1+2\rho_0 v_0 v'_{1x}+\rho_1 v_0^2)+ik\rho_0 v_0 v_{1y}=\rho_1 g-\gamma^2\xi\rho_0 , \tag{A2}$$

the momentum equation along the unperturbed front as

$$\gamma\rho_0 i v_{1y}+\rho_0 v_0\frac{di v_{1y}}{ds}=k\left[\rho_1 T_0+\rho_0 T_1-\xi\frac{d}{ds}(\rho_0 T_0)\right] , \tag{A3}$$

and the energy equation as

$$\begin{aligned}\gamma[\tfrac{3}{2}(\rho_1 T_0+\rho_0 T_1)+\tfrac{1}{2}\rho_1 v_0^2+\rho_0 v_0 v'_{1x}]-[\rho_0(v'_{1x}+\gamma\xi)+\rho_1 v_0]g-\gamma\xi\frac{d}{ds}[\tfrac{3}{2}\rho_0 T_0+\tfrac{1}{2}\rho_0 v_0^2]\\ +\frac{d}{ds}[\rho_0 v_0(\tfrac{5}{2}T_1+v_0 v'_{1x})+(\rho_1 v_0+\rho_0 v'_{1x})(\tfrac{5}{2}T_0+\tfrac{1}{2}v_0^2)]+ik\rho_0 v_{1y}(\tfrac{5}{2}T_0+\tfrac{1}{2}v_0^2)\\ =\frac{d}{ds}[(\rho_0 T_0)^{-\mu}\frac{d}{ds}(\bar{K}T_0^n T_1)]-k^2(\rho_0 T_0)^{-\mu}\bar{K}T_0^n T_1+\frac{k^2\xi}{n+1}(\rho_0 T_0)^{-\mu}\frac{d}{ds}(\bar{K}T_0^{n+1})\\ -\frac{\mu}{n+1}\frac{d}{ds}\left[\frac{(\rho_1 T_0+\rho_0 T_1)}{(\rho_0 T_0)^{1+\mu}}\frac{d}{ds}(\bar{K}T_0^{n+1})\right] .\end{aligned} \tag{A4}$$

The entropy equation may be more convenient to use sometimes instead of Eq. (A4):

$$\rho_0 T_0\left[\left(\gamma+v_0\frac{d}{ds}\right)\left(\frac{3}{2}\frac{T_1}{T_0}-\frac{\rho_1}{\rho_0}\right)+v'_{1x}\frac{d}{ds}\ln\frac{T_0^{3/2}}{\rho_0}\right]+(\rho_1 T_0+\rho_0 T_1)\left(\frac{\partial}{\partial t}+v_0\frac{\partial}{\partial s}\right)\ln\frac{T_0^{3/2}}{\rho_0}=\Phi_1 , \tag{A5}$$

where Φ_1 represents the left hand side of Eq. (A4).

APPENDIX B

$$a_1=\begin{bmatrix} 0 & 0 & \frac{-1}{\eta^{1/n}} & 0 & 0\\ \frac{-2}{n\eta^{1-1/n}} & 0 & 1 & \frac{1}{\eta^2} & \frac{-1}{\eta}\\ 0 & 1 & 0 & 0 & 0\\ 0 & 0 & 0 & 0 & 1\\ \frac{1}{n^2\eta^{1-1/n}} & 0 & 0 & 1-\frac{1}{n\eta^2} & \frac{1}{n\eta} \end{bmatrix} , \tag{B1}$$

$$a_2=\begin{bmatrix} 0 & 0 & 0 & \frac{1}{\eta^{1+2/n}} & 0\\ -1 & 0 & 0 & \frac{-2}{\eta} & 0\\ 0 & 0 & \frac{-1}{\eta^{1/n}} & 0 & 0\\ 0 & 0 & 0 & 0 & 0\\ 0 & 0 & 0 & \frac{1}{n\eta^{1+1/n}} & 0 \end{bmatrix} , \tag{B2}$$

$$a_3=\begin{bmatrix} 0 & 0 & \frac{6+5(n-\mu)}{5(n+1)} & 0 & 0 \\ \frac{\sigma_1}{\eta^{1-2/n}} & \frac{1}{n\eta^{1-1/n}} & \eta^{1/n} & \frac{2n-1}{n\eta^{2-1/n}} & \frac{-1}{\eta^{1-1/n}} \\ 0 & 0 & 0 & 0 & 0 \\ 0 & 0 & 0 & 0 & 0 \\ \frac{\sigma_2}{\eta^{1-2/n}} & \frac{1+\mu}{n^2\eta^{1-1/n}} & \sigma_3\eta^{1/n} & \frac{\sigma_4}{\eta^{2-1/n}} & \frac{\sigma_5}{\eta^{1-1/n}} \end{bmatrix}, \tag{B3}$$

where the σ_j coefficients depend on the constants n,μ entering in the model of the energy transport law:

$$\sigma_1=\frac{-2(17+15n-10\mu)}{5n(n+1)},$$
$$\sigma_2=-\frac{26+25n+5\mu(1+2n)}{5(1+n)n^2},$$
$$\sigma_3=\frac{1-5\mu+(1+n)(8+5\mu)}{5n(1+n)},$$
$$\sigma_4=\frac{n(10\mu+8)-3}{5n^2}+\frac{(1-5\mu)(1+2n)}{5(1+n)},$$
$$\sigma_5=-\left[\frac{4(5\mu+2)}{5n}+\frac{3(1-5\mu)}{5(1+n)}\right],$$
$$b_1=\left\{0,0,\frac{1}{n\eta^{1-1/n}},0,-\frac{\eta^{1/n}}{n}\right\},\quad b_2=\{0,0,0,0,0\},$$
$$b_3=\left\{0,0,\frac{2[6+5(n-\mu)]}{5n(1+n)\eta^{1-2/n}},0,\frac{-2(1-5\mu)}{5n}\eta^{2/n}\right\}.$$

APPENDIX C

In this Appendix we give the solution of Eqs. (76)–(78) near $\eta=0^+$ and match the solution that is emerging from region 2. Let $w_j\equiv\{F_j,P_j,V_j,\eta\Theta_j,d(\eta\Theta_j)/d\eta\}$, where $j=1,2,3,\ldots,$

$$\begin{aligned} F_1&\approx f_1-\eta-\frac{q_1 n}{2n-1}\eta^{(2n-1)/n}+\cdots, \\ P_1&\approx q_1-\frac{f_1(2n+1)}{n}\eta^{1/n}+\cdots, \\ V_1&\approx q_1\eta+\eta^{1/n}+\cdots, \\ \Theta_1&\approx\frac{f_1}{n}\eta^{1/n}-\frac{\eta^{(n+1)/n}}{2n}+\cdots, \end{aligned} \tag{C1}$$

$$\begin{aligned} F_2&\approx f_2+\frac{(n+f_1)}{n-1}\eta^{(n-1)/n}+\cdots, \\ P_2&\approx q_2-\frac{f_2(2n+1)}{n}\eta^{1/n}+\cdots, \\ V_2&\approx -1+q_2\eta-\frac{(2n+1)}{n+1}f_2\eta^{(n+1)/n}+\cdots, \\ \Theta_2&\approx\frac{f_2}{n}\eta^{1/n}+\frac{(1+f_1)}{(n-1)(2n-1)}\eta+\cdots, \end{aligned} \tag{C2}$$

$$\begin{aligned} F_3&\approx f_3-\eta-\frac{q_3 n}{2n-1}\eta^{(2n-1)/n}+\cdots, \\ P_3&\approx q_3-\left[\frac{f_3+\mu q_1}{n}+\frac{f_1(2n+1)}{n}\right]\eta^{1/n}+\cdots, \\ V_3&\approx\frac{6+5(n-\mu)}{5(n+1)}\eta^{1/n}+q_3\eta\cdots, \\ \Theta_3&\approx\frac{(f_3+\mu q_1)}{n}\eta^{1/n}+\frac{2f_1(1-5\mu)}{5n}\eta^{2/n}\cdots. \end{aligned} \tag{C3}$$

APPENDIX D

In order to impose on Eqs. (76)–(78) as a boundary condition the fact that the solution has to be bounded at $\eta\to\infty$, it is crucial to know analytically the behavior of its homogeneous solution for $\eta\to\infty$. It is convenient in order to get the equations in the standard form to make the change of variable $\tilde{F}=\eta^{1/n}F$, and hence the homogeneous solution of Eqs. (76)–(78) verifies the following fifth order differential system:

$$\frac{d\mathbf{V}}{d\eta}=A\mathbf{V},$$

where

$$A=\begin{bmatrix} \frac{1}{n\eta} & 0 & -1 & 0 & 0 \\ \frac{-2}{n\eta} & 0 & 1 & \frac{1}{\eta^2} & \frac{-1}{\eta} \\ 0 & 1 & 0 & 0 & 0 \\ 0 & 0 & 0 & 0 & 1 \\ \frac{1}{n^2\eta} & 0 & 0 & 1-\frac{1}{n^2\eta} & \frac{1}{n\eta} \end{bmatrix}.$$

We next expand in general $A=\sum_{j=0}^{j=\infty}A_j\eta^{-j}$ and $\mathbf{V}=\sum_{j=0}^{j=\infty}\mathbf{V}_j\eta^{-j}$. Let $\hat{P}$ be a nonsingular matrix that diagonalizes A_0 (we are assuming the existence of five independent eigenvectors) and we make $\mathbf{V}=\hat{P}\cdot\mathbf{W}$ and write the above equation as

$$\frac{d\mathbf{W}}{d\eta}=B\mathbf{W},\quad\text{where } B\equiv\hat{P}^{-1}A\hat{P}=\sum_{j=0}^{j=\infty}B_j\eta^{-j}.$$

We attempt a formal solution of the type

$$\mathbf{W}=\eta^{\alpha}\exp(\lambda\eta)\sum_{k=0}^{k=\infty}\mathbf{W}_k\eta^{-k},$$

and substituting into the above equation we formally obtain

$$\sum_k \lambda \mathbf{W}_k \eta^{-k} + \sum_k (\alpha - k)\mathbf{W}_k \eta^{-(k+1)} = \sum_{j,k} B_j \mathbf{W}_k \eta^{-(j+k)} \tag{D1}$$

and collecting terms

$$(B_0 - \lambda I)\cdot \mathbf{W}_0 = 0 , \tag{D2}$$

$$(\alpha - i + 1)\mathbf{W}_{i-1} - \sum_{\substack{j,k \\ j+k=i}} B_j \mathbf{W}_k = (B_0 - \lambda I)\mathbf{W}_i , \quad i \geq 1 , \tag{D3}$$

where I is the unit matrix.

As may be shown A_0 has five linearly independent eigenvectors and the five eigenvalues are ± 1 (double) and 0. Let μ_0 represent one such eigenvalue and let ω_0 be the corresponding eigenvector for B_0.

For the eigenvalue $\mu_0 = 0$ (simple root), taking $\lambda = \mu_0$ and $\mathbf{W}_0 = \omega_0$, we satisfy Eq. (D2), while for $i = 1$ Eq. (D3) becomes

$$(\alpha I - B_1)\omega_0 = (B_0 - \lambda I)\mathbf{W}_1 , \tag{D4}$$

and left hand multiplying (D4) by ω_0 gives the compatibility condition that determines α,

$$\omega_0 \cdot (\alpha I - B_1)\cdot \omega_0 = 0 ; \tag{D5}$$

then (D4) will give us $\mathbf{W}_1$ except one component of it, which is determined in the following order $i = 2$:

$$[(\alpha - 1)I - B_1]\mathbf{W}_1 - B_2 \omega_0 = (B_0 - \lambda I)\mathbf{W}_2 , \tag{D6}$$

and left hand multiplying (D6) by ω_0 gives the compatibility condition that determines the unknown component of $\mathbf{W}_1$:

$$\omega_0 \cdot [(\alpha - 1)I - B_1]\cdot \mathbf{W}_1 - \omega_0 \cdot B_2 \cdot \omega_0 = 0 , \tag{D7}$$

and (D7) will determine $\mathbf{W}_2$ except one component of it, which is determined in the following order $i = 3$, and so on.

This procedure must be modified at the first step if there are double roots. Let μ_0 represent one such eigenvalue $+1$ or -1 and ω_0^I, ω_0^{II} its two independent eigenvectors of B_0 for the double eigenvalue μ_0. Obviously $\mathbf{W}_0 = \beta_I \omega_0^I + \beta_{II}\omega_0^{II}$ satisfied (D2), with β_I and β_{II} being arbitrary constants. For $i = 1$ the following equation must be satisfied:

$$(\alpha I - B_1)(\beta_I \omega_0^I + \beta_{II}\omega_0^{II}) = (B_0 - \lambda I)\mathbf{W}_1 , \tag{D8}$$

and left hand multiplying by ω_0^I and ω_0^{II} gives

$$\begin{aligned} &\omega_0^I \cdot (\alpha I - B_1)\cdot (\beta_I \omega_0^I + \beta_{II}\omega_0^{II}) = 0 , \\ &\omega_0^{II} \cdot (\alpha I - B_1)\cdot (\beta_I \omega_0^I + \beta_{II}\omega_0^{II}) = 0 . \end{aligned} \tag{D9}$$

The homogeneous system in β_I and β_{II} has a different trivial solution if

$$\begin{aligned} &[\omega_0^I \cdot (\alpha I - B_1)\cdot \omega_0^I]\cdot [\omega_0^{II}\cdot (\alpha I - B_1)\cdot \omega_0^{II}] \\ &\quad - [\omega_0^I \cdot (\alpha I - B_1)\cdot \omega_0^{II}]\cdot [\omega_0^{II}\cdot (\alpha I - B_1)\cdot \omega_0^I] = 0 . \end{aligned} \tag{D10}$$

Equation (D10) gives us two solutions for α and, finally, with (D9) we get a relation between β_I and β_{II} and hence Eq. (D8) will determine $\mathbf{W}_1$ except one component of it, which is obtained in the following order $i = 2$. The procedure is easily followed for $i = 3, 4, \ldots$, and so on.

In the following we summarize the first terms of the solution $\mathbf{V}$ as $\eta \to \infty$. The calculations were performed using a symbolic compiler as MATHEMATICA [32]: Modes I–II: $[\mu_0 = -1, \alpha = (3 \pm \sqrt{5})/4n]$:

$$\eta^{(3+\sqrt{5})/(4n)} \exp(-\eta) \left[\begin{bmatrix} 1 \\ -1 \\ 1 \\ \dfrac{-2}{n(1+\sqrt{5})} \\ \dfrac{2}{n(1+\sqrt{5})} \end{bmatrix} + O(\eta^{-1}) \right] ,$$

$$\eta^{(3-\sqrt{5})/(4n)} \exp(-\eta) \left[\begin{bmatrix} 1 \\ -1 \\ 1 \\ \dfrac{-2}{n(1-\sqrt{5})} \\ \dfrac{2}{n(1-\sqrt{5})} \end{bmatrix} + O(\eta^{-1}) \right] .$$

Mode III ($\mu_0 = 0$, $\alpha = -1/n$):

$$\eta^{-1/n} \left[\begin{bmatrix} 1 \\ 0 \\ 0 \\ 0 \\ 0 \end{bmatrix} + \eta^{-1} \begin{bmatrix} 0 \\ 0 \\ \dfrac{2}{n} \\ \dfrac{-1}{n^2} \\ 0 \end{bmatrix} + \eta^{-2} \begin{bmatrix} \dfrac{4 + 8/n + 3/n^2}{2n} \\ \dfrac{-2(n+1)}{n^2} \\ 0 \\ 0 \\ \dfrac{1+n}{n^3} \end{bmatrix} + O(\eta^{-3}) \right] .$$

Modes IV–V [$\mu_0=1$, $\alpha=(3\pm\sqrt{5})/4n$]:

$$\eta^{(3-\sqrt{5})/(4n)}\exp(\eta)\left[\begin{bmatrix}1\\-1\\-1\\\dfrac{2}{n(1-\sqrt{5})}\\\dfrac{2}{n(1-\sqrt{5})}\end{bmatrix}+O(\eta^{-1})\right],$$

$$\eta^{(3+\sqrt{5})/(4n)}\exp(\eta)\left[\begin{bmatrix}1\\-1\\-1\\\dfrac{2}{n(1+\sqrt{5})}\\\dfrac{2}{n(1+\sqrt{5})}\end{bmatrix}+O(\eta^{-1})\right].$$

The eigenvalues q_j, f_j were calculated up to $O(\eta^{-2})$ terms in the IV–V modes. Such terms are not given here due to the extension of the expressions. We point out that a correct determination of modes IV–V is crucial in order to impose correctly the boundary conditions at $\eta\approx\infty$.

[1] G. Taylor, Proc. R. Soc. London A **201**, 192 (1950); S. Chandrasekar, *Hydrodynamic and Hydromagnetic Stability* (Oxford University Press, Oxford, England, 1961), Chap. 10.

[2] J. S. Shiau, E. B. Goldman, and C. I. Werg, Phys. Rev. Lett. **32**, 352 (1974).

[3] S. E. Bodner, Phys. Rev. Lett. **33**, 761 (1974).

[4] M. Tabak, D. H. Munro, and J. D. Lindl, Phys. Fluids B **2**, 1007 (1990); J. H. Gardner, S. E. Bodner, and J. P. Dahlburg, *ibid.* **3**, 1070 (1991); J. D. Kilkenny, Bull. Am. Phys. Soc. **34**, 2040 (1989).

[5] J. Grun, M. E. Emery, C. K. Manka, T. N. Lee, E. A. McLean, A. Mostovych, J. Stamper, S. Bodner, S. P. Obenschain, and B. H. Ripin, Phys. Rev. Lett. **58**, 2672 (1987); M. Desselberger, O. Willi, M. Savage, and M. J. Lamb, *ibid.* **65**, 2997 (1990); M. Desselberger and O. Willi, Phys. Fluids B **5**, 896 (1993).

[6] L. Baker, Phys. Fluids **21**, 295 (1978); W. H. Manheimer and D. G. Colombant, *ibid.* **27**, 983 (1984); H. J. Kull and S. I. Anisimov, *ibid.* **29**, 2067 (1986).

[7] H. Takabe, K. Mima, L. Montierth, and R. L. Morse, Phys. Fluids **28**, 3676 (1985).

[8] H. J. Kull, Phys. Fluids B **1**, 170 (1989).

[9] V. V. Bychkov, S. M. Golberg, and M. A. Liberman, Phys. Fluids B **5**, 3822 (1993); Phys. Plasmas 1, **9**, 2976 (1994).

[10] A. B. Bud'ko and M. A. Liberman, Phys. Rev. Lett. **68**, 178 (1992).

[11] B. A. Remington, S. W. Haan, S. G. Glendinning, J. D. Kilkenny, D. H. Munro, and R. J. Wallace, Phys. Rev. Lett. **67**, 3259 (1991); B. A. Remington, S. W. Haan, S. G. Glendinning, J. D. Kilkenny, D. H. Munro, and R. J. Wallace, Phys. Fluids B **4**, 967 (1992); B. A. Remington, S. V. Weber, S. W. Haan, J. D. Kilkenny, S. G. Glendinning, R. J. Wallace, W. H. Goldstein, B. G. Wilson, and J. K. Nash, *ibid.* **5**, 2589 (1993); S. V. Weber, B. A. Remington, S. W. Haan, B. G. Wilson, and J. K. Nash, Phys. Plasmas **11**, 3652 (1994).

[12] A. I. Akhiezer, I. A. Akhiezer, R. V. Polovin, A. G. Sitenko, and K. N. Stepanov, *Plasma Electrodynamics. Vol. 1: Linear Theory* (Pergamon, New York, 1975).

[13] M. A. Liberman, V. V. Bychkov, S. M. Goldberg, and D. L. Book, Phys. Rev. E **49**, 445 (1994).

[14] M. Van Dyke, *Perturbations Methods in Fluid Mechanics* (Academic, New York, 1964).

[15] J. Sanz, Phys. Rev. Lett. **73**, 2700 (1994).

[16] G. D. Tsakiris and K. Eidmann, J. Quant. Spectrosc. Radiat. Transfer **38**, 353 (1987).

[17] L. Spitzer, *Physics of Fully Ionized Gases* (Wiley, New York, 1962).

[18] *Enrico Fermi. Collected Papers* (University of Chicago, Chicago, 1965).

[19] D. L. Book, Plasma Phys. Controlled Fusion **34**, 737 (1992).

[20] L. D. Landau, Acte Physicochim. URSS **17**, 77 (1944); Zh. Eksp. Teor. Fiz. **14**, 240 (1944).

[21] J. G. Wouchuk and A. R. Piriz, Phys. Plasmas **2**, 493 (1995).

[22] R. Betti, R. L. McCrory, and C. P. Verdon, Phys. Rev. Lett. **71**, 3131 (1993).

[23] J. Sanz, J. A. Nicolas, J. R. Sanmartin, and J. Hilario, Phys. Fluids **31**, 2320 (1988).

[24] L. Sirovich, *Techniques of Asymptotic Analysis* (Springer-Verlag, New York, 1971).

[25] J. Sanz, A. Liñán, M. Rodriguez, and J. R. Sanmartin, Phys. Fluids **24**, 2098 (1981).

[26] W. Kruer, Plasma Phys. **5**, 69 (1979).

[27] C. E. Max, C. F. McKee, and W. C. Mead, Phys. Fluids **23**, 1620 (1980); J. Sanz and J. R. Sanmartin, *ibid.* **26**, 3361 (1983).

[28] W. M. Manheimer and D. G. Colombant, Phys. Fluids **25**, 1644 (1982).

[29] J. Sanz, Plasma Phys. Controlled Fusion **30**, 1813 (1988); J. Sanz and A. Estevez, Laser Part. Beams **9**, 273 (1991); J. Sanz and F. Minotti, Plasma Phys. Controlled Fusion **34**, 353 (1992).

[30] R. Betti, V. N. Goncharov, R. L. McCrory, and C. P. Verdon, Phys. Plasmas **2**, 3844 (1995).

[31] R. Ramis, R. Schmaltz, and J. Meyer-ter-Vehn, Comput. Phys. Commun. **49**, 475 (1988).

[32] *Mathematica, A System for Doing Mathematics by Computer* (Addison-Wesley, New York, 1991).